THE JOURNAL OF PHYSICAL CHEMISTRY B

Article

pubs.acs.org/JPCB

An Extensible Framework for Capturing Solvent Effects in Computer Generated Kinetic Models

Amrit Jalan, Richard H. West,† and William H. Green*

Department of Chemical Engineering, Massachusetts Institute of Technology, 77 Massachusetts Avenue, Cambridge, Massachusetts 02139, United States

Supporting Information

ABSTRACT: Detailed kinetic models provide useful mechanistic insight into a chemical system. Manual construction of such models is laborious and error-prone, which has led to the development of automated methods for exploring chemical pathways. These methods rely on fast, high-throughput estimation of species thermochemistry and kinetic parameters. In this paper, we present a methodology for extending automatic mechanism generation to solution phase systems which requires estimation of solvent effects on reaction rates and equilibria. The linear solvation energy relationship (LSER) method of Abraham and co-workers is combined with Mintz correlations to estimate $\Delta G^{\circ}_{solv}(T)$ in over 30 solvents using solute descriptors estimated from group additivity. Simple corrections are found to be adequate for the treatment of radical sites, as suggested by comparison with known experimental data. The performance of scaled particle theory expressions for enthalpic−entropic decomposition of $\Delta G^{\circ}_{solv}(T)$ is also presented along with the associated computational issues. Similar high-throughput methods for solvent effects on free-radical kinetics are only available for a handful of reactions due to lack of reliable experimental data, and continuum dielectric calculations offer an alternative method for their estimation. For illustration, we model liquid phase oxidation of tetralin in different solvents computing the solvent dependence for ROO• + ROO• and ROO• + solvent reactions using polarizable continuum quantum chemistry methods. The resulting kinetic models show an increase in oxidation rate with solvent polarity, consistent with experiment. Further work needed to make this approach more generally useful is outlined.

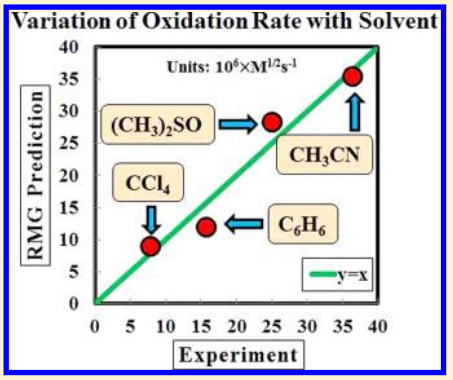

1. INTRODUCTION

Chemical kinetic models are used to simulate and understand many important systems, ranging from the metabolism of bacteria to the performance of new engine designs. Manual construction of large kinetic models is a tedious task, and it is often difficult to ensure that these models contain all important reaction pathways. This difficulty has motivated research into computer algorithms, databases, and cheminformatics tools to enable systematic construction of detailed kinetic models using computers.[1,2] Methods for automatic calculation of species thermochemistry and rate coefficients, and related database issues, are areas of intense research activity.[3] Our own efforts in this direction have led to the development of Reaction Mechanism Generator (RMG), an open-source software package for automatic mechanism generation.[4] Most existing work in automatic mechanism generation (including RMG) is focused on gas phase kinetic models with applications in understanding pyrolysis and combustion.

Solvent effects on reaction rates have been studied for over a century starting with the Menschutkin reaction.[5,6] Over the past century, solvent effects on reaction kinetics (especially ionic reactions) have been widely studied experimentally and theoretically.[6] However, solvents can also affect free-radical reactions[7] like those that occur in industrially important liquid phase hydrocarbon autoxidation. Important applications include oxidation of cyclohexane, the products of which are used in the synthesis of nylon-6 and nylon-6,6; oxidation of *p*-xylene to yield terephthalic acid, a key building block of poly ethylene terephthalate; and cumene oxidation to obtain cumene hydroperoxide, used to produce phenol.[8,9] The formation of engine and fuel injector deposits is also believed to originate from autoxidation of liquid fuel and lubricants. Polymer aging and atherosclerosis are other processes where free radical chemistry in the solution phase plays an important role.[10] Detailed kinetic models of these processes can provide useful mechanistic details about the underlying chemistry. However, the complexity associated with condensed phase systems makes this a formidable task. The work of Pfaendtner and Broadbelt[11,12] on the autoxidation of octane and decane in the liquid phase is among the few available applications of automatic mechanism generation to a liquid phase system but does not include any explicit corrections for the presence of the solvent. Similarly, solvent effects have also been of considerable interest in the coal liquefaction/resid cracking community,[13,14] but most modeling studies exclude explicit treatment of solvent effects on thermochemistry and kinetics. Recently Jorgensen

Received: November 1, 2012
Revised: January 4, 2013
Published: January 9, 2013

and co-workers[15,16] have published methods for predicting solvent effects on elementary reaction steps using QM/MM methods with applications in synthetic chemistry. However, none of the existing tools provides a systematic way to automatically incorporate solvent effects on elementary reaction rates and equilibria in a detailed kinetic model.

In this paper, we present and validate an extensible framework for automatic mechanism generation in solution phase using the linear solvation energy relationship (LSER) approach for thermodynamics and kinetics, in addition to diffusion limits on reaction rates. The next section introduces the Reaction Mechanism Generator (RMG) software which also provides insight into the tools required to extend this concept to solution phase systems. Following this, we present a detailed discussion of solvation thermodynamics with emphasis on the LSER approach, its implementation, and validation using experimental data. Next, we discuss methods to estimate solvent effects on kinetics and diffusive limits of reaction rates. Finally, for illustrative purposes, we use these methods to build kinetic models of tetralin autoxidation in different solvents.

2. PRINCIPLES OF AUTOMATED MECHANISM GENERATION

Reaction Mechanism Generator (RMG)[4,17,18] is an automated gas phase mechanism building tool that employs state-of-the-art methods in cheminformatics, thermochemistry, and kinetic parameter estimation. RMG has been demonstrated to build accurate kinetic models for pyrolysis and oxidation of several hydrocarbons.[19,20] Recent advances in RMG's development include improved estimates of pressure-dependent rates and methods for improving thermo-chemical estimates of cyclic species.[21]

RMG follows a rate-based algorithm[22] for the construction of chemical kinetic models for a given set of reactants and initial conditions (temperature, pressure, species concentration). Chemical species are represented and manipulated using graph theory tools and methods. Each species in the chemical model is classified as a *core* or *edge* species and transferred from the edge to the core when the species flux exceeds a critical value (characteristic flux, R_{char}) set by a user specified tolerance (ϵ). The species in the reactive core are allowed to react with each other using various reaction *templates*. On the basis of the enumerated reactions and their respective fluxes, the core and the edge are expanded and the process is repeated. At each step in model development, the resulting differential equations for all the species in the core (based on the current mechanism) are solved. The process continues until a user specified termination criterion is achieved.

Implementation of this algorithm requires on-the-fly estimation of thermo-chemical and kinetic parameters for thousands of species and reactions. Kinetic parameters are required to estimate the forward rates of reactions, while thermo-chemical data are used to compute the equilibrium constants required for the reverse rate coefficients. Current *ab initio* methods for performing such calculations are not fast enough to be employed at such a large scale, and simplified empirical schemes that are amenable to high-throughput estimation are used instead. RMG uses Benson's group additivity method for the estimation of gas phase thermochemistry ($H(T)$, $G(T)$, $S(T)$, $C_p(T)$) along with suitable corrections for open shell species. Rate constants are estimated using rate rules for the Arrhenius parameters (A and E_a) of different reaction families. In some cases, Evans–Polanyi relations between the activation energy (E_a) and the standard state enthalpy of reaction (ΔH°_{rxn}) are employed to estimate the activation energies. Rate rule parameters for the reaction families are obtained from experimental data or generated using *ab initio* calculations for a set of representative reactions. This framework allows RMG to quickly estimate thermo-chemical and kinetic parameters at each step of model generation.

Extension of RMG to solution phase systems requires analogous methods for estimating thermochemistry and rate coefficients in the solvents of interest. However, this task is complicated by the multitude of solvents that one may be interested in modeling and the many different solvent properties that a reaction may be sensitive to. In principle, it is possible to construct group additivity schemes and reaction rate rules exclusively for a few solvents of interest, but this task requires fitting different sets of functional group values and kinetic parameters for different solvents. It is highly desirable to employ a methodology that is extensible and allows one to switch between multiple solvents with ease, both for species thermochemistry and reaction rates. The linear free energy relationship (LFER) approach to solvation, described in the following section, has many such features that make it an attractive option for application to automatic mechanism generation in different solvents.

3. HIGH-THROUGHPUT ESTIMATION OF SOLUTION PHASE THERMOCHEMISTRY

The free energy change associated with the process of transferring a molecule from the gas phase to the solvent phase is defined as the free energy of solvation (ΔG°_{solv}). Many different methods have been developed for computing solvation energies among which continuum dielectric and force field based methods are popular. Theoretical methods for computing ΔG°_{solv} are the subject of several review articles.[23−27] Not all of these methods are easy to automate, and many are not robust, i.e., they either fail or give unreasonable results for certain solute−solvent pairs. CPU time and memory (RAM) requirements are also important considerations for kinetic modeling where thermochemistry estimates for tens of thousands of species may be required for model building (see case studies presented in later parts). Thus, we need methods which take seconds rather than hours of CPU time to compute each ΔG°_{solv} value. A fairly accurate and fast method for computing ΔG°_{solv} is the LSER approach described below.

3.1. LSERs and the Abraham Model. Linear solvation energy relationships (LSERs) provide a route for estimating properties of a solute−solvent system using multiparameter equations derived from fitting against experimental data. In this approach, both the solute and the solvent are characterized by *molecular descriptors*.[28] The most general form of an LSER can be written as[29]

$$\text{solvation energy related property}\ (F) = c_{solvent} + \sum_i p_i^{solvent} P_i^{solute} \quad (1)$$

where the index i denotes a specific solute−solvent interaction modeled as the product of a solute descriptor (P_i^{solute}) and a solvent descriptor ($p_i^{solvent}$). Descriptors characterize the tendency of the solute/solvent to participate in a specific interaction. Descriptors can also be viewed as coefficients of a first-order Taylor expansion, where $p_i^{solvent} = (\partial F/\partial P_i^{solute})_{P_{ref}}$ and $c_{solvent} = F_{ref}(\text{real}) - \sum_i p_i^{solvent} P_{i,ref}$.

dx.doi.org/10.1021/jp310824h | J. Phys. Chem. B 2013, 117, 2955−2970

The Abraham LSER provides an estimate of the partition coefficient (more specifically, the log (base 10) of the partition coefficient) of a solute between two solvents ($K_{solvent-solvent}$) or between the vapor phase and a particular solvent ($K_{vapor-solvent}$) (also known as gas−solvent partition coefficient) at 298 K. The mathematical form of the Abraham model differs depending on whether the quantity being estimated is $K_{solvent-solvent}$ or $K_{vapor-solvent}$, as shown below:

$$\log_{10} K_{solvent-solvent} = c + eE + sS + aA + bB + vV \quad (2)$$

$$\log_{10} K_{vapor-solvent} = c + eE + sS + aA + bB + lL \quad (3)$$

The Abraham model can be used to estimate ΔG°_{solv} which is related to the $K_{vapor-solvent}$ of a solute according to the following expression:

$$\Delta G^\circ_{solv} = -RT \ln K_{vapor-solvent} \quad (4)$$

$$= -2.303RT \log_{10} K_{vapor-solvent} \quad (5)$$

Recently, the validity of eq 5 has been the subject of some debate.[30,31] However, eq 5 and the conditions at which it is valid can be obtained from thermodynamic considerations alone and are listed below: (1) The gas phase behaves ideally at the equilibrium and standard state concentrations. (2) The solute is infinitely dilute at the equilibrium and standard state concentrations. A correction factor is required if different standard state concentrations are used for the different phases. These conditions can be derived using equilibrium thermodynamic expressions for solution phase systems.[32] Please see the Supporting Information for details.

The variables in the Abraham model represent solute (*E*, *S*, *A*, *B*, *V*, *L*) and solvent descriptors (*c*, *e*, *s*, *a*, *b*, *v*, *l*) for different interactions. The *sS* term is attributed to electrostatic interactions between the solute and the solvent (dipole−dipole interactions related to solvent dipolarity and the dipole−induced dipole interactions related to the polarizability of the solvent).[24,25,33] The *lL* term accounts for the contribution from cavity formation and dispersion (dispersion interactions are known to scale with solute volume[24,33]). The *eE* term, like the *sS* term, accounts for residual contributions from dipolarity/polarizability related interactions for solutes whose blend of dipolarity/polarizability differs from that implicitly built into the *S* parameter.[24,25,34] The *aA* and *bB* terms account for the contribution of hydrogen bonding between the solute and the surrounding solvent molecules. H-bonding interactions require two terms, as the solute (or solvent) can act as acceptor (donor) and vice versa. The descriptor *A* is a measure of the solute's ability to donate a hydrogen bond (acidity), and the solvent descriptor *a* is a measure of the solvent's ability to accept a hydrogen bond. A similar explanation applies to the *bB* term.[24,33,35]

Substantial work has been done to develop a physical understanding of the solute descriptors (*A*, *B*, *E*, *L*, *S*) and relate them to fundamental molecular properties[36−39] (for a recent review, see ref 25). The solvent descriptors (*c*, *e*, *s*, *a*, *b*, *l*) are largely treated as regressed empirical coefficients. Very recently, Hoffmann et al.[40] have shown that the solvent descriptors can also be correlated with solvent properties derived from quantum calculations. Detailed descriptions of the Abraham model and the descriptors employed are available in many reviews on the subject.[24,25,33,35,41] LSERs like the Abraham model are powerful tools for organizing large amounts of experimental solvation data into easily employable analytical forms.

3.2. Group Additivity Method for Estimation of Abraham Solute Descriptors. Group additivity is a convenient way of estimating the thermochemistry for thousands of species sampled in a typical mechanism generation job. Use of the Abraham model in RMG requires a similar approach to estimate the solute descriptors (*A*, *B*, *E*, *L*, and *S*) (the *V* descriptor is not required for $K_{vapor-solvent}$). Platts et al. proposed such a scheme employing a set of 81 molecular fragments for estimating *B*, *E*, *L*, *V*, and *S* and another set of 51 fragments for the estimation of *A*. Statistical significance of the fragment contributions was verified through the *t*-test.[42] Of all the fragments defined by Platts et al., only those containing C, H, and O were employed in the present work (shown in the Supporting Information) in order to match RMG's existing capabilities. Fragments defined to capture interactions between groups/substituents were not employed in the present work. The value of a given descriptor for an arbitrary molecule was obtained by summing the contributions from each fragment found in the molecule and the intercept associated with that descriptor. Once the solute descriptors were estimated, the partition coefficients ($K_{vapor-solvent}$) and the free energies of solvation were estimated using the equations discussed earlier. Solvent descriptors required for these calculations were obtained from existing literature sources.[33]

3.3. Decomposition of ΔG°_{solv} into Enthalpic and Entropic Contributions. The Abraham/Platts method provides estimates of ΔG°_{solv} at room temperature only, i.e., 298 K. The temperature dependence of ΔG°_{solv} and its molecular origins are not well understood for most nonaqueous solvents. However, a simple approximation for $\Delta G^\circ_{solv}(T)$ is to break up $\Delta G^\circ_{solv}(298)$ into enthalpic and entropic terms and use eq 6. In this section, we discuss different methods to perform this enthalpic−entropic split.

$$\Delta G^\circ_{solv}(T) \approx \Delta H^\circ_{solv}(298\ \mathrm{K}) - T\Delta S^\circ_{solv}(298\ \mathrm{K}) \quad (6)$$

3.3.1. Scaled Particle Theory (SPT) for Estimating ΔS°_{solv}. Pierotti[27] proposed analytical expressions for estimating the free energy of cavity formation (ΔG_{cav}) as a function of temperature (T), pressure (P), solute/solvent radii ($r_{solvent}$, r_{solute}), and solvent density (ρ). These expressions (shown below) are also used in many continuum solvation models[23] to estimate ΔG_{cav}.

$$\Delta G_{cav} = K_0 + K_1 r_{cav} + K_2 r_{cav}^2 + K_3 r_{cav}^3 \quad (7)$$

$$K_0 = RT\left[-\ln(1-y) + \frac{9}{2}\left(\frac{y}{1-y}\right)^2\right] - \frac{4\pi P}{3} r_{solvent}^3 \quad (8)$$

$$K_1 = -\frac{RT}{2r_{solvent}}\left[6\left(\frac{y}{1-y}\right) + 18\left(\frac{y}{1-y}\right)^2\right] + 4\pi P r_{solvent}^2 \quad (9)$$

$$K_2 = \frac{RT}{4r_{solvent}^2}\left[12\left(\frac{y}{1-y}\right) + 18\left(\frac{y}{1-y}\right)^2\right] + 4\pi P r_{solvent} \quad (10)$$

$$K_3 = \frac{4}{3}\pi P \quad (11)$$

dx.doi.org/10.1021/jp310824h | J. Phys. Chem. B 2013, 117, 2955−2970

$$y = \frac{4\pi\rho r_{solvent}^{3}}{3} \quad (12)$$

In their study on aqueous hydroxylamine chemistry, Ashcraft et al.[32] employed Pierotti's expressions to estimate the entropy change upon cavity formation using $\Delta S_{cav} = -(\partial \Delta G_{cav}/\partial T)_P$ from which one obtains

$$\Delta S_{cav} = K_0' + K_1' r_{cav} + K_2' r_{cav}^{2} \quad (13)$$

where $r_{cav} = r_{solute} + r_{solvent}$ and $K_i' = -(\partial K_i/\partial T)_P$. Parameters like ρ and possibly also $r_{solvent}$ and r_{solute} depend on temperature, so this derivative can be complicated. For the solvents and solutes considered in this work, we neglect the temperature dependence of ρ, $r_{solvent}$, and r_{solute}.

This method is useful if the required solute and solvent parameters can be estimated without much computational effort. An implicit assumption here is that a reliable estimate of ΔS_{cav} should be able to account for a bulk of the loss in total entropy, ΔS°_{solv}. This may be a reasonable assumption in apolar, aprotic solvents like n-alkanes but may lead to errors in solvents like water[32] and alcohols where hydrogen bonding plays an important role.

The use of solute radii in solvation modeling is discussed in detail elsewhere,[23] and different methods for estimation of such radii have been proposed. It is desirable that the method adopted in RMG be easily implementable, possibly using a group additivity model. One method is to derive effective radii using molecular volumes of the species estimated using UNIFAC functional groups and volume contributions associated with them.[43,44] A second method uses the McGowan volume V,[35,45] also used as a solute. McGowan's volume is also used as a solute descriptor in the Abraham model for solvent−solvent partitioning. In any case, we treat the solute as a perfect sphere with the effective radius estimated using $r_{solute} = (3V/4\pi)^{1/3}$. For this work, we only use the McGowan method since results are qualitatively similar with the UNIFAC method. Other input parameters like solvent density (ρ) can be obtained from standard property tables for most important solvents. The solvent radius ($r_{solvent}$) was obtained using volumes estimated using the *volume* keyword in Gaussian 03.[32] Estimates of the radii for some solvents can be obtained directly from the Gaussian 03 PCM software package; we used these when available.

3.3.2. Mintz Correlations for Estimating ΔH°_{solv}. Recently, Mintz et al.[46−53] have developed linear correlations similar to the Abraham model for estimating the enthalpy change associated with solvation (ΔH°_{solv}) with the objective of providing a measure of the temperature dependence of partition coefficients obtained at room temperature.

$$\Delta H^{\circ}_{solv}(298\ \mathrm{K}) = c' + a'A + b'B + e'E + s'S + l'L \quad (14)$$

where A, B, E, S, and L are the same solute descriptors used in the Abraham model for the estimation of ΔG°_{solv}. The lowercase coefficients c', a', b', e', s', and l' depend only on the solvent and were obtained by fitting to experimental data. The contribution from the L term in eq 14 may seem surprising, given that the cavity formation process it represents is largely entropic. However, as noted by Vitha and Carr,[24] the L descriptor also implicitly accounts for some dispersion interactions which scale with the volume of the solute species. Combining the Mintz and Abraham models with Platts' group additivity method for estimating solute descriptors provides a way to estimate $\Delta G_{solv}(T)$ for most solutes in many solvents using eq 15

$$\Delta G^{\circ}_{solv}(T) \approx \Delta H^{\circ}_{solv}(298) - \frac{T}{298}(\Delta H^{\circ}_{solv}(298) - \Delta G^{\circ}_{solv}(298)) \quad (15)$$

where $\Delta H^{\circ}_{solv}(298)$ is given by eq 14 and $\Delta G^{\circ}_{solv}(298)$ by eqs 3 and 5.

4. VALIDATION OF THE LSER APPROACH FOR ESTIMATING ΔG°_{solv}

The proposed method for fast estimation of ΔG°_{solv} involves three approximations: neglect of the T dependence of ΔH°_{solv} and ΔS°_{solv}, use of the Abraham/Mintz LSER approach to estimate $\Delta H^{\circ}_{solv}(298)$ and $\Delta S^{\circ}_{solv}(298)$, and the use of Platts' group additivity method to estimate solute descriptors that go into these LSERs. For purposes of kinetic modeling, it is important to quantify the performance of these methods for species in our domain of interest (relatively simple species containing C, H, and O).

Platts et al. performed a preliminary validation of their group additivity approach using it to estimate partition coefficients between water and other solvents (octanol, cyclohexane, and chloroform).[42] The solutes in both these studies were complex, multifunctional species including moieties like halogens, sulfur, phosphorus, and nitrogen. The predictions of the water−octanol partition coefficients were not particularly encouraging. It should be noted that several group contribution approaches have been developed specifically for the water−octanol partition coefficient (also known as log P), as this quantity is widely used as a descriptor in medicinal chemistry.[54] The performance of the general purpose Platts' method was expectedly worse than some of these more specialized methods.

In another recent study, Schuurmann et al.[55] implemented the Platts fragment model and pointed out several inconsistencies with the formulation of the fragments as well as issues with the actual interpretation of some of the groups. However, none of the inconsistencies reported by Schuurmann et al. apply to the C, H, and O groups employed in the present work. Schuurmann et al. proposed methods to address some of these issues and applied the modified version to the estimation of the gas−water partition coefficient (K_{aw}) and soil sorption coefficients (K_{oc}). As in the study of Platts et al., Schuurmann et al. compared the Platts method to others developed exclusively for the estimation of K_{aw} and K_{oc}. Estimates from the fragment approach were found to be in significant error compared to the experimental values. Schuurmann et al. also performed calculations with a subset of the original data set corresponding to compounds with experimental Abraham descriptors. The resulting improvements in the fits with this subset led Schuurmann et al. to claim that these models work only in the restricted domain of their training sets. Since our domain of interest is significantly different from the solutes used in prior studies, we performed our own validation described below.

4.1. Experimental Data: Minnesota Solvation Database. Experimental data for validation of RMG's estimates was obtained from the MNSOL database of Truhlar and co-workers.[56] Only neutral solutes containing C, H, and O with $\Delta G^{\circ}_{solv}(298)$ measured in solvents with known Abraham parameters were used for validation. The resulting test set contains 935 data points spanning 119 solutes and 35 solvents.

dx.doi.org/10.1021/jp310824h | J. Phys. Chem. B 2013, 117, 2955−2970

The solutes in the test set comprise many different species classes like alkanes, alkenes, alcohols, acids, ethers, esters, lactones, as well as cyclic and aromatic species. Data on the solute descriptors estimated using Platts' groups and the solvent descriptors used for the calculations are summarized in the Supporting Information. The solvation energies used in the test data set were in the 0−14 kcal/mol range (in this set, all $\Delta G^{\circ}_{solv} < 0$). Refer to the Supporting Information and the MNSOL manual for details.

4.2. Comparison of RMG Estimates with MNSOL. Platts' fragments were organized into RMG readable graph theory representations, while solvent descriptors were stored and read in from a database as required. The resulting $\log_{10} K_{vapor-solvent}$ values were converted into ΔG°_{solv} using eq 5.

The comparison between RMG's estimates of $\Delta G^{\circ}_{solv}(298\ K)$ and the experimental values over the entire test set is shown in Figure 1. The root mean squared error (RMSE) of RMG's

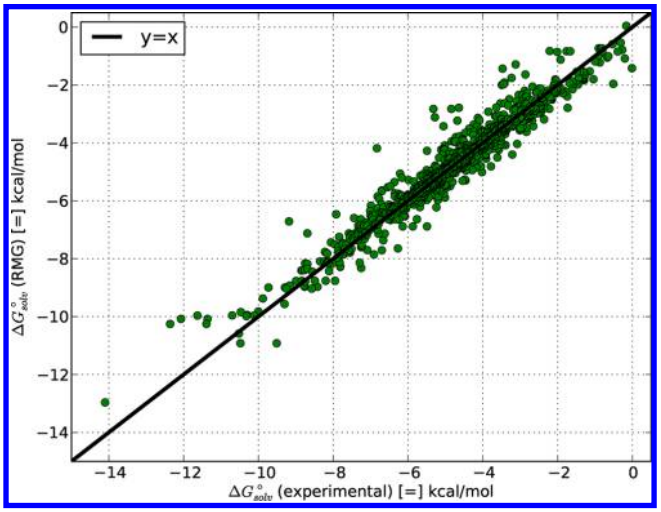

Figure 1. Comparison of $\Delta G^{\circ}_{solv}(298\ K)$ estimates from RMG with experimental values.

estimates was found to be 0.47 kcal/mol. In some cases, the discrepancy was as high as 3 kcal/mol which can lead to significant errors in estimates of reaction equilibria for kinetic modeling. Identifying outliers is important for building and improving models that use these estimates. For this purpose, solvents in the test data set were classified into two categories corresponding to strong and weak H-bonding solvents (for an example, see Table 1). Comparisons with experimental data for the weak and strong H-bonding solvents are shown in the Supporting Information. The RMSE for strong H-bonding solvents was found to be 0.70 kcal/mol, while that for weak H-bonding solvents was 0.30 kcal/mol. Similar trends were also observed by Schuurmann et al.[55]

Table 1. Solvent Abraham "*a*" and "*b*" Parameters for a Few Sample Solvents

solvent	*a*	*b*	category
water	3.904	4.814	strong
octanol	3.56	0.702	strong
dimethyl sulfoxide (DMSO)	5.46	0.0	strong
hexane	0.0	0.0	weak
benzene	0.457	0.169	weak
carbon disulfide	0.027	0.095	weak

The Abraham/Platts approach only applies to stable species, as it uses experimental data to fit LSER correlations. Experimental data on solvation thermodynamics of radical intermediates is scarce because of their inherent instability, and the few data points available are mainly for aqueous systems. There have been some attempts to estimate Abraham-like parameters for individual free radical intermediates.[57,58] The approach adopted in RMG for radical intermediates was to use the descriptors of the corresponding saturated species as a starting point. For carbon-centered radicals, the descriptors of the parent species were used without any modifications. For oxygen-centered radicals, the descriptor *A* which accounts for the acidity was corrected by subtracting the contribution of the −OH group to account for the missing H on the radical site. Using this approximation for the HO• and HOO• radicals in water at 298 K, we obtain $\Delta G^{\circ}_{solv}(298)$ estimates of −4.7 and −7.5 kcal/mol, respectively, which are in reasonable agreement with the experimental values −3.9[59] and −6.8 kcal/mol.[60] See the Supporting Information for details. We also tested the performance of the Abraham/Platts method on the SAMPL blind data sets[61,62] proposed recently to test the predictive capabilities of solvation models. Results for the SAMPL0 and SAMPL1 are available elsewhere.[25] The RMSE of the Abraham/Platts predictions on the latest SAMPL2 data set[63] was 2.33 kcal/mol, and a comparison with other methods tested on the same data set is shown in Table 2. Similar to

Table 2. Performance of Various Predictive Solvation Approaches on the SAMPL2 Data Set[a]

method	RMSE (kcal/mol)
all-atom MD (Mobley)	2.73
FiSH (Purisima)	2.24
COSMO-RS (Klamt)	1.56
ZAP (Nicholls and Ellingson)	2.17
Abraham/Platts (*Absolv*)	2.33

[a]The present work uses the Abraham/Platts method.

previous SAMPL challenges, the performance of the Abraham/Platts approach is comparable and in some cases better than other more sophisticated models. The main outliers in the Abraham/Platts approach belong to the halo-uracil family of compounds (5-bromouracil, 5-chlorouracil, 5-fluorouracil, 5-iodoracil, 6-chlorouracil), and the RMSE of this family alone was close to 3 kcal/mol. The *Absolv* module in the ADME package (ver. 4.95) was used to estimate the hydration free energies in the SAMPL2 data set to handle elements (e.g., halogens and phosphorus) not implemented in RMG. RMG and *Absolv* estimates for $\Delta G^{\circ}_{solv}(298)$ on the MNSOL test set were found to be in good agreement. Please see the Supporting Information for data on individual species in the SAMPL2 data set.

The comparison with the MNSOL database should be treated as a test of reproducibility, since the species in the test set were most likely also used to obtain the experimental descriptors used in the Platts training set. The hydration free energies in the SAMPL data sets, which were not made available until after Platts et al. developed their group values, are a better test of predictive ability and show that this method can provide estimates with errors comparable to more computationally expensive treatments. Further improvement in accuracy would obviously be helpful, and the SAMPL challenges help diagnose areas of improvement. Overall, the

dx.doi.org/10.1021/jp310824h | J. Phys. Chem. B 2013, 117, 2955−2970

comparisons above demonstrate the applicability of the Abraham/Platts approach as a tool for high-throughput estimation of $\Delta G^\circ_{solv}(298)$ for kinetic modeling. The errors in the predicted ΔG°_{solv} are of similar magnitude to errors in RMG estimates of gas-phase $\Delta G^\circ_{formation}$.

5. DECOMPOSITION OF ΔG°_{solv} INTO ΔH°_{solv} AND ΔS°_{solv}

The purpose of breaking down ΔG°_{solv} into ΔH°_{solv} and ΔS°_{solv} is to estimate ΔG°_{solv} away from the standard state temperature (298 K) implicit in the estimates obtained from the Abraham/Platts approach. In this section, issues related to the implementation of potential methods for performing this decomposition are discussed with an emphasis on input parameters and accuracies.

5.1. Sensitivity of Scaled Particle Theory (SPT) Estimates to Molecular Radii. The experimental ΔH°_{solv} data collected by Mintz et al. can be used for validating the SPT approach for ΔS°_{solv} with the following approximation:

$$\Delta H^\circ_{solv}(\mathrm{SPT})(298\ \mathrm{K}) = \Delta G^\circ_{solv}(\mathrm{Platts})(298\ \mathrm{K}) + 298\Delta S^\circ_{solv}(\mathrm{SPT})(298\ \mathrm{K}) \quad (16)$$

where the Abraham/Platts estimate of ΔG°_{solv} is used as the "experimental" value. For heptane and other alkane solvents, the ΔG°_{solv} estimates from RMG can be assumed to be reliable on the basis of the agreement with experimental data in the MNSOL data set (RMSE = 0.30 kcal/mol). We chose heptane as a model nonpolar solvent and used a test set of 99 ΔH°_{solv} values from a recent compilation by Mintz et al.[52] The IEFPCM solvent radius of heptane was used (3.125 Å), and the density at 298 K (0.684 g/cm^3) was obtained from the NIST Chemistry Webbook.[64] The resulting ΔH°_{solv} estimates with the default inputs are shown in Figure 2 (red dots).

The comparison in Figure 2 shows how ΔH°_{solv} estimates obtained from SPT expressions and default parameters are significantly inaccurate with a RMSE greater than 5 kcal/mol which can lead to large errors in $\Delta G^\circ_{solv}(T)$ estimation. Cavity formation energies obtained from SPT expressions have been shown to be sensitive to input parameters, especially solute and solvent radii,[65] and similar behavior for derivatives of ΔG°_{solv} is not surprising. Solvation models like PCM which also use this method typically rescale atomic radii to better reproduce experimental data. We tested the sensitivity of the current estimates to input radii by assigning scaling factors α and β such that $r_{solute} = r^\circ_{solute} + \alpha$ and $r_{solvent} = \beta r^\circ_{solvent}$ (all radii and α in Å, β is dimensionless). The correction factors α and β were optimized to minimize the RMSE between the experimental and theoretical estimates of ΔH°_{solv}.

The scaled values (α = −1.54 Å, β = 0.96) were found to significantly improve agreement between theory and experiment (RMSE = 0.51 kcal/mol), as shown in Figure 2 (blue dots). Similar improvements in ΔH°_{solv} estimates were also observed for other alkane-like solvents shown in Figure 3a (optimal α and β shown in Table 3). For comparison, the performance of the Mintz models for alkane solvents considered above is shown in Figure 3b using solute descriptors estimated by RMG. Comparison of Figure 3a and 3b suggests that both methods agree for nonpolar, aprotic solvents like alkanes. Problems associated with protic solvents where specific interactions can play an important role are discussed next.

5.2. Importance of Specific Interactions. The SPT expressions are based on a hard-sphere model of the solute and

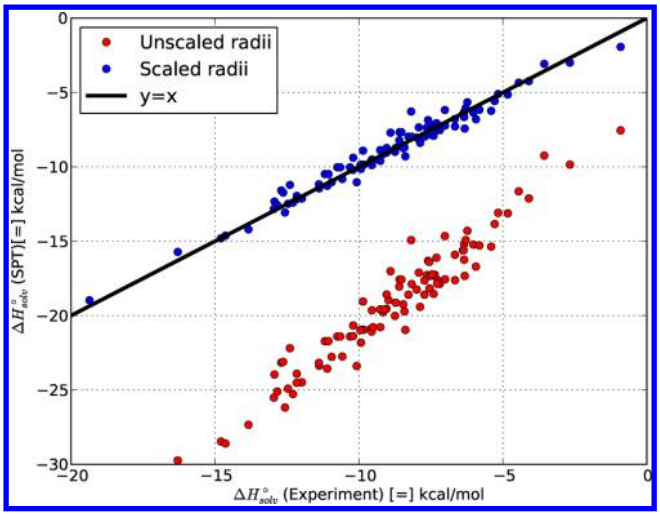

Figure 2. ΔH°_{solv} estimates (298 K) for heptane using eq 16 using scaled and unscaled radii.

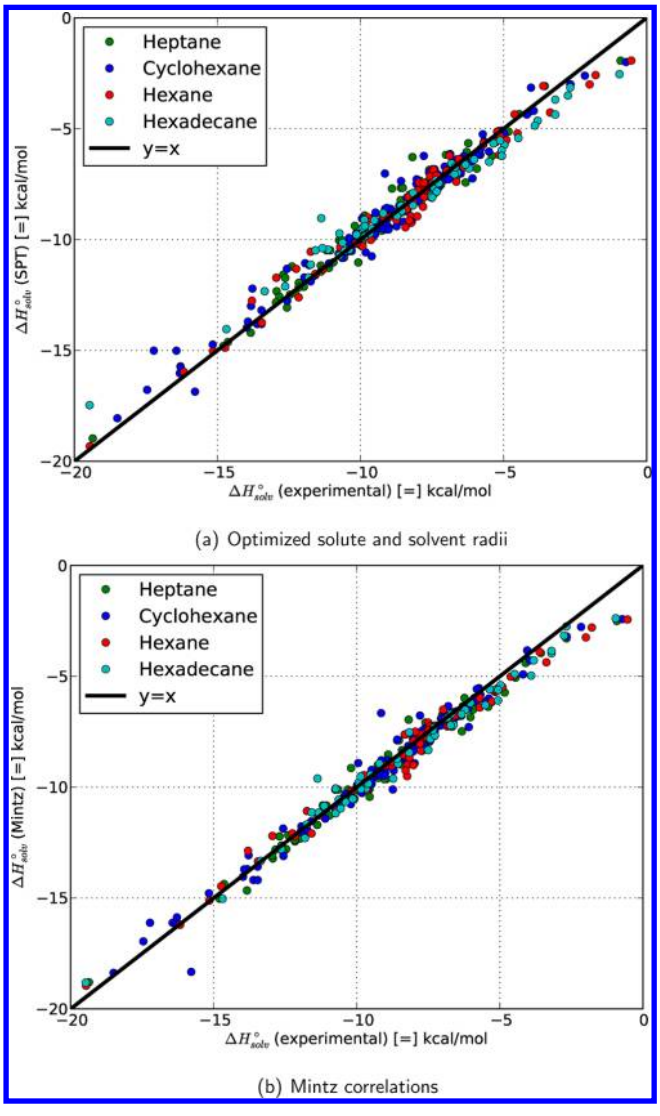

Figure 3. Comparison of ΔH°_{solv} estimates (298 K) for alkane solvents using (a) the SPT method with optimized radii and (b) Mintz correlations with RMG descriptors. These methods are comparably accurate for alkane and cycloalkane solvents.

dx.doi.org/10.1021/jp310824h | J. Phys. Chem. B 2013, 117, 2955−2970

Table 3. Optimal Values of α and β Coefficients for Alkane Solvents

solvent	$r^{\circ}_{solvent}$ (Å)	α (Å)	β
cyclohexane	2.82	−1.09	0.93
heptane	3.13	−1.54	0.96
hexane	3.12	−1.61	0.99
hexadecane	4.80	−1.48	0.88

the solvent.[66] As a result, the application of this model to solvation thermodynamics is limited to the cavity formation process and the energy cost associated with it. In reality, the solvation process also includes specific interactions like hydrogen bonding which can contribute significantly in protic solvents like alcohols and water, where hard sphere models may be inadequate. Empirical models like the Mintz correlations are capable of handling such solvents using experimental data and Abraham solute descriptors.

To better understand the effect of specific interactions on thermodynamic quantities like ΔH°_{solv}, consider octanol (as solvent) which is known to have strong H-bonding tendencies (see Table 1). Figure 4 shows the ΔH°_{solv} estimates obtained

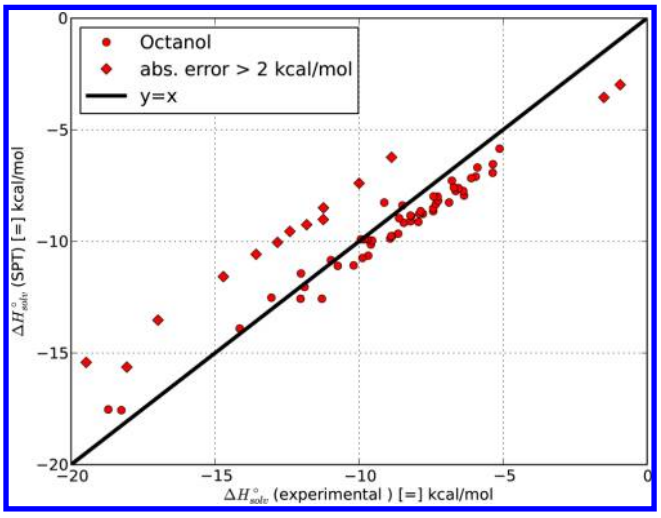

Figure 4. ΔH°_{solv} estimates in octanol solvent using the SPT model with optimized radii.

from eq 16 for 68 solutes in octanol using solute radii from the McGowan method, an initial solvent radius of 3.7 Å, and a density at 298 K of 0.824 g/cm^3. Experimental data for these comparisons were obtained from the work of Mintz et al.[46] Similar to the alkane solvents, the original parameter set gives poor estimates (RMSE > 5 kcal/mol, not shown), while those based on optimized radii (using α = 0.00 Å and β = 0.91) shown in Figure 4 are in much better agreement with experimental values (RMSE = 1.5 kcal/mol). Note that, even with optimized radii, there are significantly large outliers (absolute error >2 kcal/mol) in the parity plot of Figure 4. These correspond to alcohol solutes which have high hydrogen bond donating tendencies (large values of the descriptor A). This confirms that, in cases where specific interactions like H-bonding are important, hard sphere models can lead to erroneous estimates of ΔH°_{solv} even with empirical corrections to the input parameters.

There are two potential sources of error in ΔH°_{solv}(SPT) (eq 16): one arising from ΔG°_{solv}(298) (Abraham/Platts) and the other from assuming $\Delta S_{solv} \approx \Delta S_{cav}$. For each of the outliers in Figure 4, the estimated ΔG°_{solv}(298) closely matches the experimental value (see the Supporting Information). Thus, the discrepancy in Figure 4 arises because the hard sphere ΔS_{cav} is a poor estimate for alcohol solutes in octanol with deviations up to 5 cal/(mol-K). The failure of assuming $\Delta S_{solv} \approx \Delta S_{cav}$ for situations with H-bonding was noted previously by Ashcraft et al.[32] in aqueous systems.

The observations made with octanol also apply to other H-bonding solvents. Figure 5a shows results for dimethylsulfoxide

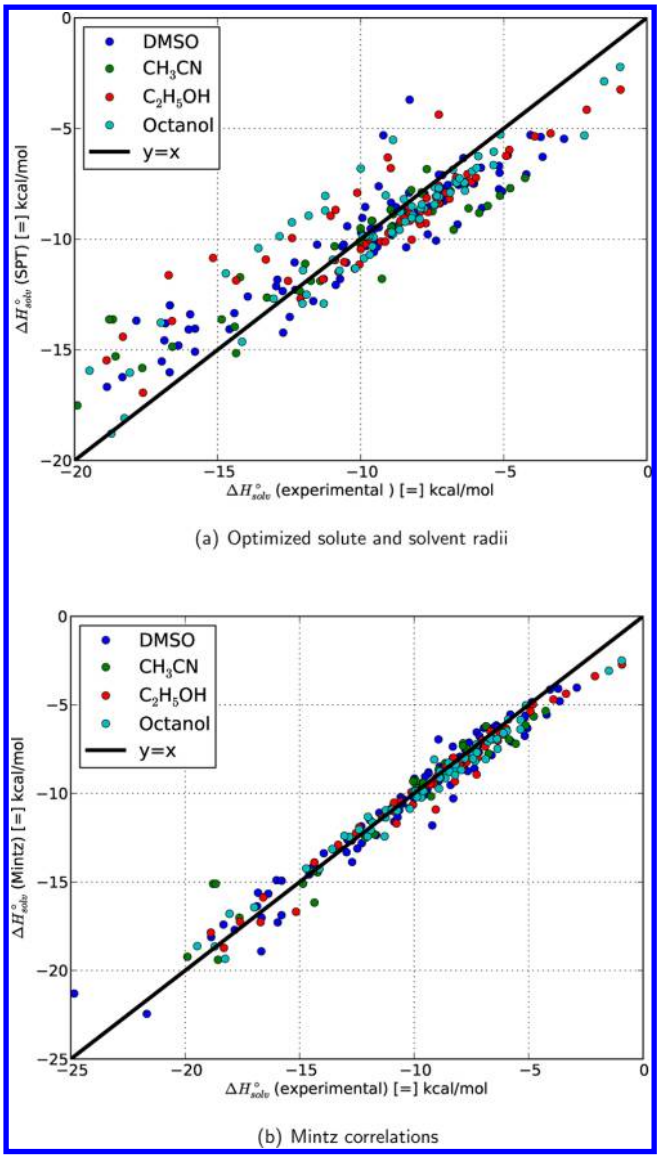

Figure 5. Comparison of ΔH°_{solv} estimates (298 K) for alkane solvents using (a) the SPT method with optimized radii and (b) Mintz correlations with RMG descriptors.

(DMSO), ethanol (C_2H_5OH), and acetonitrile (CH_3CN) in addition to octanol. The experimental data for these comparisons were obtained from the work of Mintz et al.[47,51,67] As with octanol, species with strong H-bonding tendencies were found to be major outliers even with optimal α and β for all solvents. The optimal values of α and β are shown in Table 4; the RMSE was ~2.0 kcal/mol for each H-bonding solvent.

dx.doi.org/10.1021/jp310824h | J. Phys. Chem. B 2013, 117, 2955−2970

Table 4. Optimal Values of α and β Coefficients for Protic Solvents

solvent	$r^{\circ}_{solvent}$ (Å)	α (Å)	β
DMSO	2.46	0.37	0.76
acetonitrile	2.16	2.36	0.55
ethanol	2.18	−0.24	0.86
octanol	3.70	0.00	0.78

The performance of the Mintz correlations on the same data set using solute descriptors estimated by RMG is much better (shown in Figure 5b). Mintz's empirical corrections account for the H-bonding contributions to ΔH°_{solv} and are conceptually similar to bond additivity corrections (BACs) of Ashcraft et al.[32] Clearly, a limitation of the Mintz approach is that it requires collection of appropriate data and regression analysis to determine six parameters (c', e', s', a', b', l') for each solvent. Presently, Mintz correlations exist for solvents like alkanes, alcohols, water, and some aromatic solvents.[46−53,67−69]

6. AUTOMATIC ESTIMATION OF SOLVENT EFFECTS ON ELEMENTARY REACTION RATES

In addition to methods for estimating solvation thermodynamic quantities, automatic kinetic modeling also requires estimation of solvent effects on reaction rates: both transport related effects like diffusive limits and solvent effects on the intrinsic rates of elementary reactions.[70] The theory behind diffusive limits in solution phase reactions is well established,[71] and the effective rate constant of a bimolecular reaction is given as

$$k_{eff} = \frac{4\pi R\mathcal{D}k_{int}}{4\pi R\mathcal{D} + k_{int}} \quad (17)$$

where k_{int} is the intrinsic reaction rate, R is the sum of radii of the reactants, and $\mathcal{D}$ is the sum of the diffusivities of the reacting species. RMG uses the McGowan method for estimating radii (section 3.3), and diffusivities are estimated with the Stokes−Einstein equation using experimental solvent viscosities ($\eta(T)$). In reactions like

$$A \underset{k_{r,eff}}{\overset{k_f}{\rightleftharpoons}} B + C$$

the forward rate constant (k_f) can be slowed down if the reverse rate ($k_{r,eff}$) is diffusion limited, since the equilibrium constant (K_{eq}) is not affected by diffusion limitations. In cases where both the forward and reverse reaction rates are bimolecular, both diffusive limits are estimated and RMG uses the direction with the larger effect.

Kinetic solvent effects (KSEs) on intrinsic reaction rates (k_{int}) can arise from interactions between the solvent and the reactants, transition state, or products of the reaction. There is a large body of literature on such effects for ionic reactions and their correlations with solvent properties like dielectric constant, refractive index, etc.[72] Determining and understanding KSEs on nonionic free radical reactions is an active area of research[58,73,74] with potential applications in biological systems, control of oxidation, and organic syntheses. The work of Ingold and co-workers on H-abstraction reactions is among the most heavily cited experimental investigations of kinetic solvent effects on free radical reactions.[75−78] Apart from H-abstraction reactions, other free radical reactions for which kinetic solvent effects have been investigated experimentally include beta-scission of alkoxy radicals,[79,80] decarbonylation of acyl radicals,[81] and addition of radicals to alkenes.[82,83] Most investigations of kinetic solvent effects have been experimental in nature with some theoretical estimates using continuum dielectric models.[83]

Liquid phase oxidation of hydrocarbon substrates has been studied in several solvents. Howard and Ingold reported that the rate of 2,2′-azobisisobutyronitrile (AIBN) initiated oxidation of a variety of hydrocarbon substrates increased with the dielectric constant of the solvent.[84,85] Similar observations were also made later by Niki et al.[86] who studied tetralin oxidation in several solvents. Here we use tetralin oxidation in a variety of solvents as a test case for RMG.

6.1. Computational Methods. For continuum solvation calculations, gas phase geometry optimization was performed at the B3LYP/CBSB7 level of theory followed by relaxed 1D rotor scans at the B3LYP/6-31G(d) level of theory to identify lower energy conformers. The lowest energy conformers identified were then reoptimized at the B3LYP/CBSB7 level and used for single-point solvation energy calculations. ΔG^{solv}_{ES} calculations in 10 solvents spread over a wide polarity range were carried out using the IEFPCM and CPCM solvation models in Gaussian 03[87] at the HF/6-31+G* level of theory with the cavities built using the united atom topological model and radii optimized for this level of theory (UAHF).[88,89] All other parameters in these methods were retained at their default values.

For rate coefficient calculations, geometries of minima and saddle points were optimized at the B3LYP/CBSB7 level of theory, and the CBS-QB3 compound method was used for gas phase energies. Hindered rotor corrections to the partition functions were computed using the independent rotor approximation using potentials obtained from relaxed one-dimensional scans at 10° dihedral intervals at the B3LYP/6-31G(d) level starting from the minimum energy conformer. Eckart tunneling corrections were included in all rate constant calculations. The CanTherm software package[90] was used to perform all statistical mechanics and transition state theory calculations. Rates were calculated in the 298−1500 K temperature range and fitted to modified Arrhenius rate expressions ($k = A(T/1K)^n \exp(-E_a/RT)$). For solvent corrections on rates, $\Delta\Delta G^{solv}_{ES} = \Delta G^{solv}_{ES}(TS) - \sum \Delta G^{solv}_{ES}(\text{reactants})$ was computed using the methods above and a correction factor of $\exp(-\Delta\Delta G^{solv}_{ES}/RT)$ was applied to the rate coefficient at the temperature of interest. We now discuss solvent effects on the main reactions in the tetralin oxidation system.

6.2. Solvent Effects on Initiation, Propagation, and Termination Steps. *6.2.1. Initiation by AIBN.* Solvent effects on AIBN initiation have received attention due to their role in free radical polymerization.[91−93] A representative rate constant and efficiency of the initiation reaction at 338 K was obtained from the corresponding measurement of Howard and Ingold in pure styrene[84] ($ek_i = 1.5 \times 10^{-5}$ s^{-1}). Niki et al.[94] measured the rate of AIBN initiation and efficiency of radical production in various solvents at 343 K during their investigation of solvent effects on tetralin autoxidation. They concluded that the rate constant of initial decomposition of AIBN is similar in most solvents ($\sim 4 \times 10^{-5}$ s^{-1}) and that the efficiency of radical production varies inversely with the viscosity which is indicative of diffusive limitations. However, recently Makitra et al.[95] have correlated the rate of AIBN initiation with both specific and nonspecific solvation effects (eq 18), suggesting that the viscosity dependence may be an oversimplification. For kinetic modeling, we used the AIBN decomposition rates (determined

dx.doi.org/10.1021/jp310824h | J. Phys. Chem. B 2013, 117, 2955−2970

from the rate of nitrogen evolution) measured by Howard and Ingold[85] in different solvents, and assumed e = 0.75. The conditions (initial AIBN concentration and temperature) used in their work were the same as those used for the tetralin experiments that we sought to model. The AIBN initiation rate (k_i) in DMSO solvent was estimated using the Makitra correlation shown below:

$$\log_{10}\frac{k_i(65\ ^\circ\mathrm{C})}{1\ \mathrm{s}^{-1}} = -5.574 + 2.09\left(\frac{n^2-1}{n^2+2}\right) + 1.014\times10^{-3}B + 6.82\times10^{-3}E_T - 0.324\times10^{-3}\delta^2 \quad (18)$$

In eq 18, n is the refractive index, E_T is the Reichardt electrophilicity parameter, B is the Koppel−Palm basicity, and δ is the Hildebrand solubility parameter.[95,96] An extensive list of these solvent descriptors is available in the compilation by Abboud and Notario.[96]

6.2.2. Propagation: ROO• + RH. The main propagation step in tetralin oxidation involves H-atom transfer from the α position in tetralin to the α-tetralyl peroxy radical, forming the corresponding hydroperoxide. Baulch et al. have recommended Arrhenius parameters (A = 1.3 × 10^{12} cm^3/mol-s, E_a = 11.3 kcal/mol) for a closely related reaction HOO• + ethylbenzene =1-phenyl ethyl + H_2O_2 in the gas phase.[97] However, Carstensen et al.[98] have reported that abstraction rates from alkanes are higher for HOO• compared to other alkyl peroxy radicals. For this study, we assumed the propagation rate per H atom to be similar to $CH_3OO•$ + ethylbenzene = 1-phenyl ethyl + CH_3OOH and estimated rate coefficients for this reaction using CCSD(T)-F12a/VDZ-F12//B3LYP/CBSB7 energies (calculated using the Molpro software package[99]) and scaled zero-point energies from B3LYP/CBSB7 calculations. The CBS-QB3 calculations used for all other rates in this work were computationally prohibitive for this system due to the presence of 11 heavy atoms. The computed rates for $CH_3OO•$ + ethylbenzene (A = 8.7 × 10^{11} cm^3/mol-s, E_a = 13.0 kcal/mol) are a factor of 8 lower than the Baulch recommendation for HOO• + ethylbenzene at temperatures less than 500 K, consistent with the peroxyl radical reactivity trend reported by Carstensen et al.

Early studies proposed that the observed increase in oxidation rate with dielectric constant could be due to dipolar transition states involved in this step.[84,85] However, for the ROO• + RH reactions, absence of polar effects was experimentally demonstrated by Lucarini et al.[100] who performed cumene oxidation studies in different solvents and observed no significant change in the propagation rate between isooctane and polar solvents like acetonitrile, *tert*-butanol, and pyridine. However, very recent experiments[73,101,102] show polarity related effects in other H-abstraction reactions, suggesting these effects may vary from case to case. Our continuum solvation calculations for two representative reactions (Table 5) are consistent with this view. Further experimental investigation of ROO• + RH rate constants in different solvents may be required to better understand the role of dipolar effects.[74] For the purposes of tetralin oxidation, values from Table 5 for $CH_3OO•$ + $C_6H_5CH_2CH_3$ were used for the variation of k_p with the dielectric constant of the solvent.

Ingold and co-workers performed experimental measurements[76−78,103] of H-abstraction reactions in different solvents and proposed that solvent effects arise primarily from 1:1 H-bond complexation between the substrate undergoing abstraction (XH) and the solvent (S). This would lead to a decrease in the number of free sites available to the attacking radical (Y•) and a drop in the reaction rate. For a general H-abstraction reaction (Y• + XH), Snelgrove et al.[77] proposed an empirical correlation to capture this solvent dependence of the forward rate constant.

$$\log_{10} k_{solv} = \log_{10} k_0 - 8.3A_{XH}B_S \quad (19)$$

where k_0 is the rate of reaction between Y• and free (i.e., non-H-bonded) XH, A_{XH} is the H-bond donating ability (acidity) of the substrate, and B_S is the H-bond accepting ability of a single solvent molecule.[41,77] B_S should not be confused with the Abraham a parameter shown in Table 1 which measures the average H-bond accepting ability of the bulk solvent. The role of protic solvents in such reactions is unclear given that ROO• radicals are known to be good H-bond acceptors and are likely to form complexes with H-bond-donating solvents.[104]

For the ROO• + tetralin reaction, eq 19 suggests that solvent effects should be negligible, as the H-bond donating capacity of cyclo-alkanes (A_{XH}) is close to zero.[79] This was also experimentally confirmed by Lucarini et al.[100] for the cumene oxidation system in isooctane, benzene, acetonitrile, *tert*-butanol, and pyridine. However, the same is not true of the reverse reaction (R• + ROOH), since ROOH species (A = 0.348) donate H-bonds more readily than alkanes, so R• + ROOH should be slowed down in H-bond-accepting solvents. From microscopic reversibility, even though k_{solv}(ROO• + RH) is insensitive to the solvent, k_{solv}(R• + ROOH) can be solvent dependent if $K_{eq,solv}$ varies with solvent type. At room temperature, it was observed that the solvent effect predicted by Snelgrove for the R• + ROOH reaction is within a factor of 4 of the RMG prediction based on change in $K_{eq,solv}$ using the thermochemistry methods and radical corrections discussed earlier and assuming no solvent effects on the forward reaction. These calculations are summarized in Table 6 for nine solvents (at T = 298 K). For normal oxidations, the flux of the reverse reaction is many orders of magnitude smaller compared to the forward reaction as the concentrations of ROOH/R• species

Table 5. Change in Electrostatic Component of Solvation Free Energy (kcal/mol) at 298 K Going from Reactants to Transition State ($\Delta\Delta G_{ES}^{propagation} = \Delta G_{ES}^{solv}(TS) - \Delta G_{ES}^{solv}(reactants)$) for $CH_3OO•$ + $CH_3CH_2CH_3$ ⇌ CH_3OOH + $CH_3CH•CH_3$ and $CH_3OO•$ + $C_6H_5CH_2CH_3$ ⇌ CH_3OOH + $C_6H_5CH•CH_3$ Using the IEFPCM Solvation Model and Heptane as the Reference Solvent[a]

		$-\Delta\Delta G_{ES}^{propagation}$	
solvent	ϵ	$CH_3OO•$ + $CH_3CH_2CH_3$	$CH_3OO•$ + $C_6H_5CH_2CH_3$
heptane	1.9	0.0	0.0
tetrachloromethane	2.2	0.1	0.1
benzene	2.3	0.1	0.1
toluene	2.4	0.1	0.1
ether	4.3	0.5	0.2
chloroform	4.9	0.4	0.2
chlorobenzene	5.6	0.5	0.2
acetonitrile	36.6	0.8	0.3
dimethylsulfoxide	46.7	0.8	0.3
water	78.4	1.7	0.7

[a]Note that $k_{solvent}/k_{gas} = \exp(-\Delta\Delta G_{ES}^{propagation}/RT)$, and these calculations predict a small increase in k_p as ϵ increases.

dx.doi.org/10.1021/jp310824h | J. Phys. Chem. B 2013, 117, 2955−2970

Table 6. Solvent Effect on R• + ROOH Reaction Predicted by the Snelgrove Correlation[77] Compared with a Corresponding Drop in K_{eq} Predicted by RMG at 298 K[a]

solvent	B_S[b]	a_S[c]	Snelgrove correction	RMG correction
tetrachloromethane	0.00	0.00	1.00	1.00
benzene	0.14	0.457	2.5	1.4
dibutyl ether	0.42	2.626	16.3	8.2
chlorobenzene	0.42	0.364	1.8	1.3
acetonitrile	0.44	2.085	18.7	5.3
ethyl acetate	0.45[d]	2.949	19.9	10.6
tetrahydrofuran	0.51	3.289	29.7	13.0
dimethylformamide	0.66[e]	4.112	80.6	27.0
dimethylsulfoxide	0.78	5.46	179.0	79.5

[a]The Snelgrove correction factor is calculated as $10^{8.3(0.348)(B_S)}$, since the A parameter for ROOH species is 0.348. The RMG correction equals $10^{0.345a_S}$, since R• and RH have similar values for A while the value for ROO• is 0.345 lower than that for ROOH because of the missing contribution from the −OH group. [b]Values of B_S were obtained from the work of Abraham et al.[105] [c]a_S values obtained from the compilations of Abraham and co-workers.[41,106,107] [d]Value for ethyl acetate obtained from the value for the general estimate for RCO_2R in ref 105. [e]Value for DMF obtained from the value for $HCONR_2$ in ref 105.

involved are small compared to the RH/ROO• species (since the R• is trapped by O_2 under the conditions of interest). As a result, solvent effects on this rate do not have a significant impact on the final yield of ROOH.

6.2.3. Termination: ROO• + ROO•. The third important reaction type in initiated liquid phase oxidations is the bimolecular termination reaction between peroxy radicals (eq 20). According to the Russell mechanism, this reaction is believed to proceed through a tetroxide intermediate which falls apart to the final products.[108] The reaction scheme for this process is shown below:

$$2\mathrm{ROO}\bullet \underset{k_{-1}}{\overset{k_1}{\rightleftharpoons}} \mathrm{ROOOOR} \xrightarrow{k_2} \mathrm{ROH} + \mathrm{R{=}O} + \mathrm{O_2} \tag{20}$$

The overall rate of termination can be written as $k_t = (k_1k_2)/(k_{-1} + k_2)$. Assuming $k_2 \ll k_{-1}$, this expression can be simplified to

$$k_t \approx \frac{k_1k_2}{k_{-1}} = k_2K_{eq} \tag{21}$$

where $K_{eq} = k_1/k_{-1}$, the equilibrium constant for the formation of the tetroxide intermediate from the peroxy radicals.

Solvent effects on the ROO• + ROO• termination step have been proposed earlier.[100,109,110] Hendry and Russell attributed solvent effects to the polar character of the peroxy radicals which was destroyed in the termination step possibly through the tetroxide intermediate (hence affecting K_{eq} in eq 21). We confirmed this through calculations on the methyl peroxy radical ($CH_3OO\bullet$) and the corresponding tetroxide ($CH_3OOOOCH_3$) with geometries optimized at the B3LYP/CBSB7 level of theory. Indeed, the tetroxide intermediate has a much smaller dipole moment (0.50 D) compared to the two peroxy radicals (2.70 D) which leads to differences in the electrostatic component of ΔG°_{solv}. Using eqs 20 and 21, the absolute rate constant for termination in a given solvent can be written as

$$k_t = A_2 \exp\left(-\frac{E_{a,2}}{RT}\right)\exp\left(-\frac{G^{solv}_{ES,RO_4R} - 2G^{solv}_{ES,ROO\bullet}}{RT}\right) \tag{22}$$

$$= A_2K^{gas}_{eq}\exp\left(-\frac{E_{a,2} + \Delta\Delta G^{solv}_{ES}}{RT}\right) \tag{23}$$

where A_2 and $E_{a,2}$ are the Arrhenius parameters for the decomposition of the tetroxide (k_2), K^{gas}_{eq} is the equilibrium constant for the 2ROO• ⇌ RO_4R step in the gas phase. The change in effective barrier of the termination step is given by $\Delta E^{termination}_a = \Delta\Delta G^{solv}_{ES} = \Delta G^{solv}_{ES}(RO_4R) - 2\Delta G^{solv}_{ES}(ROO\bullet)$. The relation between the termination rates in solvents A and B is given by

$$RT\ln\left(\frac{k_{t,A}}{k_{t,B}}\right) = -(\Delta\Delta G^{solv}_{ES,A} - \Delta\Delta G^{solv}_{ES,B}) \tag{24}$$

For our analysis, we chose the reference solvent (B) to be pure tetralin. Representative Arrhenius parameters for the self-reaction of secondary-peroxy radicals were obtained from the measurements of Bennett[111] on the iso-propyl peroxy radical in alkane/cycloalkane solvents (A = 2.50e+12 cm^3/mol/s, E_a = 4.8 kcal/mol) in the 293−373 K temperature range using ultraviolet absorption spectroscopy to monitor the second order decay of the peroxy radicals. Experimental data on the ROO• termination step in different solvents is scarce. Recently, Lucarini et al.[100] carried out measurements for the termination rate of the cumyl peroxy radical at 323 K in isooctane, benzene,

Table 7. Change in Electrostatic Solvation Energies (kcal/mol) for Reaction ROO• + ROO• = ROOOOR for R• = Cumyl and Tetralyl Calculated Using the IEFPCM and CPCM Solvation Models

		R• = cumyl		R• = tetralyl	
solvent	ϵ	$\Delta\Delta G^{solv}_{ES,alkane}$ IEFPCM	$\Delta\Delta G^{solv}_{ES,alkane}$ CPCM	$\Delta\Delta G^{solv}_{ES,alkane}$ IEFPCM	$\Delta\Delta G^{solv}_{ES,alkane}$ CPCM
heptane	1.9	0.00	0.00	0.00	0.00
tetrachloromethane	2.2	0.08	0.05	0.09	0.08
benzene	2.3	0.08	0.07	0.09	0.09
toluene	2.4	0.16	0.13	0.16	0.14
ether	4.3	0.70	0.66	0.62	0.61
chloroform	4.9	0.52	0.46	0.50	0.45
chlorobenzene	5.6	0.64	0.57	0.58	0.54
acetonitrile	36.6	0.80	0.70	0.77	0.67
dimethylsulfoxide	46.7	0.91	0.81	0.88	0.76
water	78.4	0.62	0.51	0.56	0.40

dx.doi.org/10.1021/jp310824h | J. Phys. Chem. B 2013, 117, 2955−2970

acetonitrile, *tert*-butanol, and pyridine. The Landolt-Bornstein database reports termination rates for the cumyl peroxy radical in different solvents based on the experiments performed by Kaloerova et al.[112]

Continuum solvation calculations were performed on the gas-phase optimized geometries for the methyl peroxy ($CH_3OO\bullet$), cumyl peroxy ($C_6H_5C(CH_3)_2OO\bullet$), and tetralyl peroxy radicals and the corresponding tetroxides. The results of these calculations for the cumyl and tetralyl peroxy radicals are shown in Table 7. The results for the methyl peroxy radical are similar and are provided in the Supporting Information. As seen in Table 7, the change in the effective activation barrier predicted by these calculations relative to alkane solvents ($\Delta\Delta G^{solv}_{ES,alkane}$) for the tetralyl and cumyl peroxy radicals lies in the 0−1 kcal/mol range using both the IEFPCM and CPCM methods. Solvent effects on 2ROO• ↔ ROOOOR equilibrium were also computed using the LSER based methods discussed in section 3 and were found to be larger in magnitude than the PCM estimates (see the Supporting Information for details). However, it should be noted that Platts' group additivity method does not explicitly include peroxide linkages and we are forced to treat the O−O bonds in both ROO• and ROOOOR as a sum of −O− (ether) groups in these calculations. Because of this poor description of peroxide bonds, we use results from IEFPCM/CPCM calculations for the models in this work.

The computed ROO• termination rate correlates with the dielectric constant of the solvent according to eq 25.

$$RT\ \ln\frac{k_{solvent}}{k_{alkane}} = m\left[\left(\frac{\epsilon_{solvent}-1}{2\epsilon_{solvent}+1}\right)-\left(\frac{\epsilon_{alkane}-1}{2\epsilon_{alkane}+1}\right)\right] \quad (25)$$

where $(\epsilon - 1)/(2\epsilon + 1)$ is the Kirkwood parameter.[6] The best fit values of m for the methyl, cumyl, and tetralyl peroxy systems are shown in Table 8. These values were obtained by using the average $\Delta\Delta G^{solv}_{ES,alkane}$ of the IEFPCM and CPCM calculations shown in Table 7. The negative sign of the slope in Table 8 suggests that the rate of termination decreases with increasing dielectric constant. The predicted change in the termination rate with solvent due to the change in K_{eq} using eq 25 is in reasonable agreement with experimental observations (Figure 6). The calculated variation of k_t with solvent polarity is larger for R• = cumyl compared to R• = tetralyl.

Table 8. Values of Slope (m) (eq 25) for the Methyl, Cumyl, and Tetralyl Peroxy Systems Obtained by Fitting to $\Delta\Delta G^{solv}_{ES,alkane}$ Estimated Using PCM Calculations

ROO•	m (kcal/mol)
methyl	−2.1
tetralyl	−2.5
cumyl	−2.7

For R• = cumyl, termination rates (relative to isooctane) reported by Lucarini et al.[100] agree reasonably well with our predictions for benzene and acetonitrile (Figure 6). However, Lucarini reports an unexpected *increase* in the termination rate by factors of 1.8 and 2.4 in the very strongly H-bonding solvents, pyridine and *t*-butanol. Anomalous behavior in *tert*-butanol has also been observed in the experiments performed by Kaloereva et al.[112] and in the more recent experiments by Bietti et al.[104] on H-abstraction reactions. It is not clear if these k_t values are reliable, since one might expect changes in k_p as well in these strongly interacting solvents.

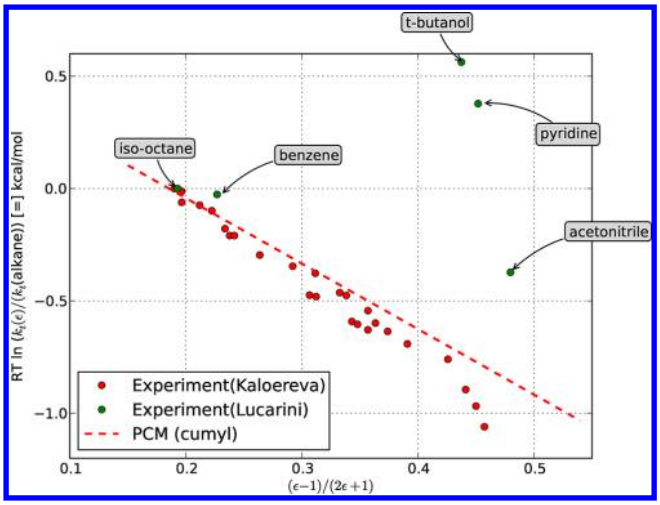

Figure 6. Variation of $RT\ln(k_{solvent}/k_{alkane})$ with solvent polarity for recombination of cumyl peroxy radicals. Experimental measurements by Kaloereva et al. (red dots) were performed at 333 K in acetic acid, decane, chlorobenzene, ethyl acetate, acetic anhydride, dimethyl sulfoxide, and *tert*-butanol. Experimental measurements by Lucarini (green dots) were performed at 323 K in iso-octane, benzene, *tert*-butanol, pyridine, and acetonitrile. Note the large discrepancy in experimental results for *t*-butanol. The dotted line is the predicted variation in K_{eq} (eq 25).

6.3. Solvent Reactivity. Solvent reactivity is an additional concern in the solvents considered here due to the high dilution of tetralin (~20). The stability of solvents like benzene and tetrachloromethane is fairly well-established, but relatively little is known about the reactivity of solvents like $CH_3C{\equiv}N$ and $CH_3S(O)CH_3$ to alkylperoxy radicals which are the main chain carriers in the present system. Previous studies on $CH_3C{\equiv}N$ and $CH_3S(O)CH_3$ have focused mainly on reactions with the hydroxyl radical.[113−116] For this study, calculations of bimolecular rate constants were performed using $CH_3OO\bullet$ as the model radical for two types of reactions: H-abstraction and addition to the double (S═O) or triple bond (C≡N). Galano[113] showed that, of the two possible addition reactions of •OH to $CH_3C{\equiv}N$, the one leading to the N-centered radical was exothermic, while the other was significantly endothermic. In the present investigation, we expected a similar trend and performed calculations for the reaction leading to the formation of the N-centered radical only.

Computed Arrhenius parameters and rates at 338 K (system temperature for oxidation experiments) are shown in Table 9. Also shown are the Arrhenius factors for the main propagation channel in which alkylperoxy radicals abstract a hydrogen from the benzylic position in tetralin. We find the addition of the $CH_3OO\bullet$ to S═O leads directly to the beta-scission products of the resulting O-centered radical much like the results of Wang et al.[115] who showed that the addition of •OH to the S═O double bond directly led to $CH_3S(O)OH$ (methane sulfinic acid) and the methyl radical. Absolute and relative rate comparisons are also shown in Table 9 with the *relative rate* accounting for the dilution (~20) used in the experimental studies. We see that, even with the dilution accounted for, at 338 K, the reactions of $CH_3OO\bullet$ with the solvents are 3 orders

dx.doi.org/10.1021/jp310824h | J. Phys. Chem. B 2013, 117, 2955−2970

Table 9. Computed Rate Coefficients for Reactions of $CH_3OO\bullet$ with Acetonitrile ($CH_3C{\equiv}N$) and Dimethyl Sulfoxide ($CH_3S(O)CH_3$) and Comparison with Propagation Channel in Tetralin Oxidation at 338 K

	reaction	A (cm^3/mol-s)	n	E_a (kcal/mol)	$\Delta\Delta G_{ES}^{\dagger,solv}$ [a] (kcal/mol)	k(338 K) [b] (cm^3/mol-s)	relative rate (338 K) [c]
1.	ROO• + tetralin ⇌ ROOH + α-tetralyl radical [d]	1.7×10^{12}	0.0	13.0	−0.1 [e]	6.8×10^{3}	1.0
2.	$CH_3OO\bullet + CH_3C{\equiv}N \rightleftharpoons CH_3OOH + \bullet CH_2C{\equiv}N$	3.7×10^{-9}	6.4	12.1	1.0 [f]	1.9×10^{-1}	2.8×10^{-5}
3.	$CH_3OO\bullet + CH_3C{\equiv}N \rightleftharpoons CH_2C(OOCH_3){=}N\bullet$	$3.1 \times 10^{+00}$	3.4	16.4	3.0 [f]	3.6×10^{-4}	5.3×10^{-8}
4.	$CH_3OO\bullet + CH_3S(O)CH_3 \rightleftharpoons CH_3OOH + CH_2S(O)CH_3$ [g]	6.9×10^{-8}	5.3	10.5	1.6 [h]	2.9×10^{-2}	4.3×10^{-6}
5.	$CH_3OO\bullet + CH_3S(O)CH_3 \rightleftharpoons CH_3\bullet + CH_3S(O)OOCH_3$	1.1×10^{-1}	3.9	16.2	2.6 [h]	5.6×10^{-4}	8.2×10^{-8}

[a] $\Delta\Delta G_{ES}^{\dagger,solv} = \Delta G_{ES}^{\dagger,solv} - \sum_i^{rxts} \Delta G_{ES}^{i,solv}$. [b] Rate coefficients are of the form $k = A(T/1K)^n \exp(-E_a/RT) \exp(-\Delta\Delta G_{ES}^{\dagger,solv}/RT)$. [c] Defined as $(20{*}k(338))/k_0(338)$ to account for experimental dilution of tetralin in solvent. [d] Reference reaction k_0 based on rate estimates for $CH_3OO\bullet + C_6H_5CH_2CH_3 \rightleftharpoons CH_3OOH + C_6H_5CH\bullet CH_3$. [e] Solvation calculations performed in heptane. [f] Solvation calculations performed in $CH_3C{\equiv}N$. [g] Solvation calculations performed in $CH_3S(O)CH_3$. [h] CBS-QB3 RRHO-TST calculation.

of magnitude slower than reactions with tetralin. Hence, only a small fraction of the tetralyl peroxy radicals generated during the oxidation will be lost by reaction with the solvents. Consequently, these solvent reactions were not included in the kinetic models.

7. KINETIC MODELING OF LIQUID PHASE AUTOXIDATION OF TETRALIN IN DIFFERENT SOLVENTS

We now present kinetic models of AIBN initiated liquid phase oxidation of tetralin[110] in different solvents built with RMG using the approximations discussed in previous sections. Generating kinetic models with RMG requires the user to specify reactant concentrations, temperature, solvent viscosity, and a termination criterion (typically reaction time or conversion of particular reactant). The models considered here were built until 3% conversion of tetralin, since we were interested in simulating early stage oxidation. A list of all the parameters for these simulations is provided in Table 10.

Table 10. Simulation Setup for Tetralin Autoxidation Models

parameter	value
tetralin concentration	7.34 M
oxygen concentration	5.43×10^{-3} M
AIBN concentration	0.01 M
temperature	65 °C
Abraham solvent parameters	cyclohexane
viscosity	1.05×10^{-3} Pa-s
species tolerance	0.01
termination criterion	3% conversion

The pure tetralin oxidation model obtained with the setup shown in Table 10 consists of 93 reactions and 29 species; for the full model, see the Supporting Information. Tightening the species tolerance from 0.01 to 0.00001 resulted in a considerable increase in mechanism size due to secondary reactions but no significant changes in the oxidation rate or main product yields. The number of core/edge species and reactions considered by RMG for progressively tighter tolerances is provided in the Supporting Information. For the remainder of this case study, the species tolerance was set at 0.01 for all RMG generated kinetic models.

α-Tetralyl hydroperoxide ($ROOH_\alpha$) (Figure 7) is the major oxidation product, and the beta-substituted isomer ($ROOH_\beta$) yield is lower by an order of magnitude. Important side products are the α-substituted isomers of tetralone ($R{=}O_\alpha$),

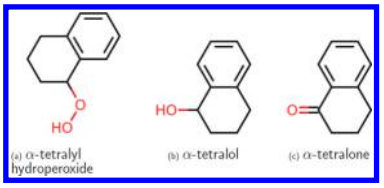

Figure 7. Important products in the liquid phase oxidation of tetralin.

tetralol (ROH_α), and water. $R{=}O_\alpha$ and ROH_α are formed mainly from the bimolecular reaction of $ROO\bullet_\alpha$ radicals which are the major chain-carrying radicals in this system. $ROO\bullet_\alpha$ is formed from the diffusion-limited recombination reaction between α-tetralyl radicals (created by reaction between radicals from AIBN and tetralin) and O_2. The main propagation channel involves reaction between $ROO\bullet_\alpha$ and tetralin to form $ROOH_\alpha$ and α-tetralyl radicals because of the weaker benzylic hydrogen. The β-abstraction channel is not entirely negligible and leads to the formation of some β-tetralyl radicals which quickly react with O_2 to give $ROO\bullet_\beta$. $ROOH_\alpha$ has a specially weak H−C(OOH) bond which can be readily abstracted to form a metastable species (•C(OOH)) which disintegrates immediately to give $R{=}O_\alpha$ and HO•. This is the main source of HO• radicals and accounts for the excess yield of $R{=}O_\alpha$ over ROH_α.

As seen in Table 11, tetralin consumption was found to be most sensitive to the rate of initiation by AIBN, H-abstraction by the $ROO\bullet_\alpha$ from tetralin, and self-reaction of $ROO\bullet_\alpha$ (Table 11). In addition, reactions 6 and 7 were also found to contribute to tetralin consumption mainly due to HO• production through reaction 4. Recently, Pfaendtner and Broadbelt[11] and Hermans et al.[9] have discussed ROO• + ROOH (reaction 4) as a route to the formation of reactive HO• radicals especially as $ROOH_\alpha$ builds up. Even with ethylbenzene as a model substrate, calculating reliable rates for these channels was not computationally affordable. We approximate this rate to be 25 times faster (per H atom at T = 338 K) than the corresponding ROO• + RH rates based on calculations performed for $CH_3OO\bullet + CH_3CH_2CH_3$ ($A = 1.3 \times 10^{-8}$ cm^3/mol-s, n = 6.2, E_a = 8.5 kcal/mol) and $CH_3OO\bullet + CH_3CH(OOH)CH_3$ ($A = 1.1 \times 10^{-13}$ cm^3/mol-s, n = 7.2, E_a = 2.9 kcal/mol) (see the Supporting Information). The data in Table 11 (reaction 4) shows that this channel has a minor contribution to tetralin consumption in the current model.

An alternative path for $ROO\bullet_\alpha$ is isomerization into the •QOOH radical via intramolecular H-migration. The •QOOH radical can then add O_2 to form •OOQOOH which subsequently forms the dihydroperoxide. Theoretical rate constants for this reaction sequence have been estimated

dx.doi.org/10.1021/jp310824h | J. Phys. Chem. B 2013, 117, 2955−2970

Table 11. Normalized Sensitivities of Tetralin $((\partial \ln[\text{tetralin}])/(\partial \ln k))$ for Pure Tetralin Oxidation at $t \approx 1.4 \times 10^4$ s (3% Conversion)

no.	reaction	sensitivity	A (cm^3/mol/s)	n	E_a (kcal/mol)	source
1.	$ROO\bullet_\alpha + RH \rightarrow ROOH_\alpha + R\bullet_\alpha$	−1.00	1.7×10^{12}	0.0	13.0	present work
2.	$ROO\bullet_\alpha + ROO\bullet_\alpha \rightarrow ROH_\alpha + R{=}O_\alpha + O_2$	0.61	2.5×10^{12}	0.0	4.8	ref 111
3.	AIBN initiation	−0.55	1.5×10^{-5}	0.0	0.0	ref 85
4.	$ROO\bullet_\alpha + ROOH_\alpha \rightarrow ROOH_\alpha + R{=}O_\alpha + HO\bullet$	−0.11	1.0×10^{13}	0.0	13.0	present work
5.	$ROO\bullet_\alpha + RH \rightarrow ROOH_\alpha + R\bullet_\beta$	−0.11	2.5×10^{-8}	6.2	8.5	present work
6.	$HO\bullet + RH \rightarrow R_\beta + H_2O$	−0.02	1.6×10^{7}	1.9	0.2	ref 117
7.	$HO\bullet + RH \rightarrow R_\alpha + H_2O$	0.02	1.7×10^{13}	0.0	2.6	ref 117

Table 12. Details of Tetralin Oxidation Models Generated Using RMG in Solvents Studied Experimentally by Howard and Ingold (T = 65°C, $[\text{AIBN}]_0$ = 0.07 M)

solvent	ϵ	viscosity $10^4 \times$ (Pa-s)	ek_i[a] $10^5 \times (s^{-1})$	$\Delta E_a^{\text{termination}}$ [b] (kcal/mol)	U_{O_2}(Expt.)[c] $10^6 \times (M^{1/2}\ s^{-1})$	U_{O_2}(RMG) $10^6 \times (M^{1/2}\ s^{-1})$
tetrachloromethane	2.23	5.5	0.9	0.09	7.9	9.0
benzene	2.25	3.7	1.4	0.09	15.8	11.9
acetonitrile	36.64	2.4	2.0	0.72	36.4	35.4
dimethylsulfoxide	46.70	11.2	1.4[d]	0.82	25.0[e]	28.3

[a]Experimental rates reported by Howard and Ingold.[85] [b]$\Delta E_a^{\text{termination}} = \Delta\Delta G_{ES,\text{alkane}}^{\text{solv}}$ from Table 7 (average of IEFPCM and CPCM values). [c]Oxygen uptake coefficient, $U_{O_2} = -(1/([\text{AIBN}]_0)^{1/2})(dO_2/dt)$, $[\text{RH}]_0$ same in all solvents. [d]Initiation rate in DMSO calculated using eq 18 and assuming e = 0.75. [e]Initial AIBN concentration used = 0.01 M.

mainly for normal and branched alkanes.[118,119] Estimates in the current model were obtained from high-pressure rate constants of Fernandes et al.[120] for the cyclohexyl + O_2 potential energy surface and did not have a major effect on the overall rate of oxidation. Traditional models of liquid phase oxidation mainly consider reactions 1, 2, and 3 in Table 11 and apply the pseudo steady-state approximation on $ROO\bullet_\alpha$ which gives $(d[O_2]/dt) = -[\text{RH}](k_p[\text{AIBN}]k_i^{0.5}/k_t^{0.5})$. The oxidation rate predicted by the current model is 1.5×10^{-5} M/s in reasonable agreement with experimental measurements (2.1×10^{-5} M/s) under similar conditions. The analytical expression mentioned above gives an oxidation rate of 1.4×10^{-5} M/s, slightly lower than the current model prediction because of the missing HO• consumption channels.

Solvent effects on reaction equilibria, diffusive limits, and solvent corrected rates for initiation and termination were combined for building oxidation models in the solution phase. Solvents chosen for these simulations were tetrachloromethane (CCl_4), acetonitrile ($CH_3C{\equiv}N$), dimethylsulfoxide ($(CH_3)_2SO$), and benzene (C_6H_6), since these were studied experimentally by Howard and Ingold[84,85] and had readily available Abraham/Mintz parameters required by RMG. Table 12 shows the effective initiation rate, viscosity, and change in effective activation barrier for the termination step (see eq 23) that were used to generate models in these solvents. The initial tetralin concentration was set at 0.37 M based on the 20-fold dilution used in the experiments of Howard and Ingold.[85] Oxygen solubilities were estimated from literature compilations.[121] Also shown in Table 12 are the experimentally observed oxygen uptake rates and those predicted by the models.

The average oxygen uptake rate in each solvent was calculated using the concentrations of the major oxidation products and time required to reach 3% conversion. The simulated oxygen uptake rates increase with solvent polarity consistent with experimental observations of Howard and Ingold as well as Niki et al.[86] The predicted absolute oxidation rates are also in good agreement with experiment. The uptake rates for each solvent in Table 12 have been scaled by the square root of the initial AIBN concentration (defined as the uptake coefficient, U_{O_2}), since the DMSO experiments were performed with $[\text{AIBN}]_0$ = 0.01 M at 65 °C, while those for the other solvents were performed with $[\text{AIBN}]_0$ = 0.07 M. The RMG generated kinetic models in each solvent were identical to that in pure tetralin with 93 reactions and 29 species. This is understandable, since the underlying chemistry remains essentially the same in inert solvents even if the main substrate is highly diluted. ROOH (α and β), $R{=}O_\alpha$, and ROH_α were the main products in all the solvents as well but with higher relative yields of $R{=}O_\alpha + ROH_\alpha$ with respect to the hydroperoxides (ROOH). This is a direct consequence of the 20-fold dilution which reduces the total flux through the propagation channels (which are proportional to [RH]) but leaves the initiation and termination channels relatively unchanged (since [AIBN] was held constant). Any flux that depends on [RH] or [ROOH] (e.g., reactions 1, 4, 5, 6, and 7 in Table 11) is reduced due to dilution. This leads to a significant drop in the amount of $R{=}O_\alpha$ formed through reaction 4, and our models predict the ketone:alcohol ratio to be close to unity at low conversions when tetralin is diluted by inert solvents. The same ratio in pure tetralin oxidation is predicted to be about 13 at 3% conversion.

8. CONCLUDING REMARKS

We have presented and discussed methods for capturing solvent effects in automatic mechanism generation using empirical correlations for both thermochemistry and kinetics refined by quantum chemistry/PCM calculations on reactions/species predicted to be most sensitive. The Abraham model combined with solute descriptors estimated from the Platts group additivity approach provides a tool for high throughput estimation of solvation free energies ($\Delta G_{\text{solv}}^{\circ}$) at room temperature across a variety of solute and solvent classes. The overall method was found to perform well over the experimental test data set obtained from the Minnesota Solvation Database (MNSOL) with a RMSE of about 0.5

dx.doi.org/10.1021/jp310824h | J. Phys. Chem. B 2013, 117, 2955−2970

kcal/mol. Solvents with strong hydrogen bonding tendencies were found to contribute to the bulk of the reported error. This method was also applied to the SAMPL2 data set to provide a measure of predictive ability. The performance of this empirical approach in estimating hydration free energies was found to be comparable to that of more sophisticated methods in the literature, in agreement with previous results for the SAMPL0 and SAMPL1 data sets reported earlier.

The temperature dependence of ΔG°_{solv} was handled by decomposing it into ΔH°_{solv} and ΔS°_{solv}. We compared two methods for performing this decomposition, one based on hard-sphere liquid theory and the other using the more recent empirical correlations developed by Mintz et al. The ΔS°_{solv} estimates from the hard-sphere model were found to be so sensitive to the molecular radii employed that to attain useful accuracy these numbers need to be empirically adjusted for each solvent. Even with adjustments, the hard-sphere model was only accurate for solvents like alkanes where specific solvation interactions are minimal. The empirical correlations of Mintz were found to accurately predict ΔH°_{solv} for both alkanes and protic solvents but require significant experimental data on each solvent of interest.

The new capability to generate kinetic models in different solvents was validated by comparing with literature experiments on tetralin oxidation. Diffusive limits were estimated automatically on all bimolecular rate constants. AIBN initiation rates in different solvents were estimated either using experimental measurements or using the Makitra correlation where rates were not available. Solvent effects on the propagation reaction (ROO• + RH) were found to be minimal. Solvent effects on the termination rate were modeled as arising from the loss of dipolarity in going from the separated peroxy radicals (ROO•) to the dimer modeled as ROOOOR. Continuum solvation calculations (PCM/CPCM) were used to estimate the magnitude of the expected solvent effect and were found to agree well with experimental observations. *Ab initio* methods were used to determine the reactivity of solvents like $CH_3C{\equiv}N$ and $CH_3S(O)CH_3$ to peroxy radicals.

Solvent effects on free radical reactions have recently attracted attention, as suggested by the increasing number of new experimental data and review articles. Recent interest in green chemistry has made it imperative to understand how solvents affect reaction kinetics and equilibria. It is also important that this understanding be put to use in developing large scale kinetic models which provide critical mechanistic insight into the role of the solvent. We hope that the methods and results presented here provide some direction toward resolving these challenges.

■ ASSOCIATED CONTENT

Supporting Information

Details of solvation energy predictions in RMG using the LSER approach, Cartesian coordinates of all stationary points discussed in the text, pure tetralin oxidation model in Chemkin format, and InChI representations of the species/intermediates in the model are provided. This material is available free of charge via the Internet at http://pubs.acs.org.

■ AUTHOR INFORMATION

Corresponding Author

*E-mail: whgreen@mit.edu.

Present Address

[†]Department of Chemical Engineering, Northeastern University, Boston, MA 02115, USA.

Notes

The authors declare no competing financial interest.

■ ACKNOWLEDGMENTS

Funding from Eni S.p.A. and the US Department of Energy (Office of Science, Office of Basic Energy Sciences, as part of the Combustion Energy Frontier Research Center under Grant Number DE-SC0001198) is gratefully acknowledged. We also thank Prof. Donald G. Truhlar for providing access to the Minnesota Solvation database (MNSOL).

■ REFERENCES

(1) Pierucci, S.; Ranzi, E. *Comput. Chem. Eng.* **2008**, *32*, 805−826.

(2) Tomlin, A. S.; Turnyi, T.; Pilling, M. J. In *Low-Temperature Combustion and Autoignition*; Pilling, M., Ed.; Comprehensive Chemical Kinetics; Elsevier B.V.: Amsterdam, The Netherlands, 1997; Vol. *35*, pp 293−437.

(3) Green, W. H. Predictive Kinetics: A New Approach for the 21st Century. In *Advances in Chemical Engineering*, Vol. *32*; Marin, G. B., Ed.; Academic Press: Burlington, MA, USA, 2007; Chapter 1, pp 2−48.

(4) Green, W. H.; et al. Reaction Mechanism Generator (RMG), version 4.0. 2013; http://rmg.sourceforge.net/.

(5) Menschutkin, N. *Z. Phys. Chem., Stoechiom. Verwandtschaftsl.* **1900**, *34*, 157−167.

(6) Reichardt, C.; Welton, T. *Solvents and Solvent Effects in Organic Chemistry*; Wiley-VCH Verlag GmbH & Co. KGaA: Weinheim, Germany, 2010; pp 165−357.

(7) Litwinienko, G.; Beckwith, A. L. J.; Ingold, K. U. *Chem. Soc. Rev.* **2011**, *40*, 2157−2163.

(8) Hermans, I.; Jacobs, P. A.; Peeters, J. *Chem.—Eur. J.* **2006**, *12*, 4229−4240.

(9) Hermans, I.; Jacobs, P.; Peeters, J. *Chem.—Eur. J.* **2007**, *13*, 754−761.

(10) Denisov, E.; Afanas'ev, I. *Oxidation and Antioxidants in Organic Chemistry and Biology*; CRC Taylor & Francis: Boca Raton, FL, USA, 2005.

(11) Pfaendtner, J.; Broadbelt, L. J. *Ind. Eng. Chem. Res.* **2008**, *47*, 2897−2904.

(12) Pfaendtner, J.; Broadbelt, L. J. *Ind. Eng. Chem. Res.* **2008**, *47*, 2886−2896.

(13) Kamiya, Y.; Futamura, S.; Mizuki, T.; Kajioka, M.; Koshi, K. *Fuel Process. Technol.* **1986**, *14*, 79−90.

(14) Ferrance, J.; Warzinski, R. P.; Bockrath, B. C. *Abstr. Pap. Am. Chem. Soc.* **1998**, *216*, U874−U874.

(15) Acevedo, O.; Jorgensen, W. L. In *Solvent Effects on Organic Reactions from QM/MM Simulations*; Spellmeyer, D. C., Ed.; Annual Reports in Computational Chemistry; Elsevier B.V.: Amsterdam, The Netherlands, 2006; Vol. *2*, Chapter 14, pp 263−278.

(16) Acevedo, O.; Jorgensen, W. L. *J. Chem. Theory Comput.* **2007**, *3*, 1412−1419.

(17) Song, J.; Raman, S.; Yu, J.; Wijaya, C. D.; Stephanopoulos, G.; Green, W. H. *Abstr. Pap. Am. Chem. Soc.* **2003**, *226*, U530−U531.

(18) Song, J.; Sumathi, R.; Yu, J.; Green, W. H. *Abstr. Pap. Am. Chem. Soc.* **2004**, *228*, U233−U233.

(19) Van Geem, K. M.; Reyniers, M. F.; Marin, G. B.; Song, J.; Green, W. H.; Matheu, D. M. *AIChE J.* **2006**, *52*, 718−730.

(20) Harper, M. R.; Geem, K. M. V.; Pyl, S. P.; Marin, G. B.; Green, W. H. *Combust. Flame* **2011**, *158*, 16−41.

(21) Magoon, G. R.; Green, W. H. *Comput. Chem. Eng.* **2012**, DOI: 10.1016/j.compchemeng.2012.11.009.

(22) Susnow, R. G.; Dean, A. M.; Green, W. H.; Peczak, P.; Broadbelt, L. J. *J. Phys. Chem. A* **1997**, *101*, 3731−3740.

(23) Tomasi, J.; Mennucci, B.; Cammi, R. *Chem. Rev.* **2005**, *105*, 2999−3094.
(24) Vitha, M.; Carr, P. W. *J. Chromatogr., A* **2006**, *1126*, 143−194.
(25) Jalan, A.; Ashcraft, R. W.; West, R. H.; Green, W. H. *Annu. Rep. Prog. Chem., Sect. C: Phys. Chem.* **2010**, *106*, 211−258.
(26) Cramer, C. J.; Truhlar, D. G. *Chem. Rev.* **1999**, *99*, 2161−2200.
(27) Pierotti, R. A. *Chem. Rev.* **1976**, *76*, 717−726.
(28) Karelson, M. *Molecular Descriptors in QSAR/QSPR*; John Wiliey and Sons, Ltd: Hoboken, NJ, USA, 2000.
(29) Cramer, C.; Truhlar, D. G. In *Quantitative Treatments of Solute/Solvent Interactions*; Politzer, P., Murray, J., Eds.; Elsevier B.V.: Amsterdam, The Netherlands, 1994; pp 9−43.
(30) Goss, K. U. *J. Phys. Chem. B* **2003**, *107*, 14025−14029.
(31) Graziano, G. *J. Phys. Chem. B* **2005**, *109*, 17768−17769.
(32) Ashcraft, R. W.; Raman, S.; Green, W. H. *J. Phys. Chem. B* **2007**, *111*, 11968−11983.
(33) Abraham, M. H.; Poole, C. F.; Poole, S. K. *J. Chromatogr., A* **1999**, *842*, 79−114.
(34) Abraham, M.; Whiting, G.; Doherty, R.; Shuely, W. *J. Chem. Soc., Perkin Trans.* **1990**, *2*, 1451−1460.
(35) Poole, C. F.; Atapattu, S. N.; Poole, S. K.; Bell, A. K. *Anal. Chim. Acta* **2009**, *652*, 32−53.
(36) Arey, J. S.; Green, W. H.; Gschwend, P. M. *J. Phys. Chem. B* **2005**, *109*, 7564−7573.
(37) Schwobel, J.; Ebert, R. U.; Kuhne, R.; Schuurmann, G. *J. Chem. Inf. Model.* **2009**, *49*, 956−962.
(38) Schwobel, J.; Ebert, R. U.; Kuhne, R.; Schuurmann, G. *J. Phys. Chem. A* **2009**, *113*, 10104−10112.
(39) Schwobel, J.; Ebert, R. U.; Kuhne, R.; Schuurmann, G. *J. Comput. Chem.* **2009**, *30*, 1454−1464.
(40) Hoffmann, E. A.; Rajko, R.; Fekete, Z. A.; Kortvelyesi, T. *J. Chromatogr., A* **2009**, *1216*, 8535−8544.
(41) Abraham, M. H.; Ibrahim, A.; Zissimos, A. M. *J. Chromatogr., A* **2004**, *1037*, 29−47.
(42) Platts, J. A.; Abraham, M. H.; Butina, D.; Hersey, A. *J. Chem. Inf. Comput. Sci.* **2000**, *40*, 71−80.
(43) Kooijman, H. A. *Ind. Eng. Chem. Res.* **2002**, *41*, 3326−3328.
(44) Fredenslund, A.; Jones, R. L.; Prausnitz, J. M. *AIChE J.* **1975**, *21*, 1086−1099.
(45) Abraham, M.; McGowan, J. *Chromatographia* **1987**, *23*, 243−246.
(46) Mintz, C.; Clark, M.; Acree, W. E.; Abraham, M. H. *J. Chem. Inf. Model.* **2007**, *47*, 115−121.
(47) Mintz, C.; Burton, K.; Acree, W. E.; Abraham, M. H. *Thermochim. Acta* **2007**, *459*, 17−25.
(48) Mintz, C.; Burton, K.; Acree, W. E.; Abraham, M. H. *Fluid Phase Equilib.* **2007**, *258*, 191−198.
(49) Mintz, C.; Clark, M.; Burton, K.; Acree, W. E.; Abraham, M. *J. Solution Chem.* **2007**, *36*, 947−966.
(50) Mintz, C.; Clark, M.; Burton, K.; Acree, W. E.; Abraham, M. *QSAR Comb. Sci.* **2007**, *8*, 881−888.
(51) Mintz, C.; Ladlie, T.; Burton, K.; Clark, M.; Acree, W. E.; Abraham, M. H. *QSAR Comb. Sci.* **2008**, *27*, 627−635.
(52) Mintz, C.; Burton, K.; Acree, W. E.; Abraham, M. *QSAR Comb. Sci.* **2008**, *27*, 179−186.
(53) Mintz, C.; Burton, K.; Ladlie, T.; Clark, M.; Acree, W. E.; Abraham, M. H. *J. Mol. Liq.* **2009**, *144*, 23−31.
(54) Mannhold, R.; Poda, G. I.; Ostermann, C.; Tetko, I. V. *J. Pharm. Sci.* **2009**, *98*, 861−893.
(55) Schuurmann, G.; Ebert, R. U.; Kuehne, R. *Chimia* **2006**, *60*, 691−698.
(56) Marenich, A.; Kelly, C.; Thompson, J.; Hawkins, G.; Chambers, C.; Giesen, D.; Winget, P.; Cramer, C.; Truhlar, D. Minnesota Solvation Database-version 2009; University of Minnesota, Minneapolis, 2009, http://comp.chem.umn.edu/mnsol/.
(57) Warren, J. J.; Mayer, J. M. *Proc. Natl. Acad. Sci. U.S.A.* **2010**, *107*, 5282−5287.
(58) Foti, M. C.; Sortino, S.; Ingold, K. U. *Chem.—Eur. J.* **2005**, *11*, 1942−1948.
(59) Roeselova, M.; Vieceli, J.; Dang, L. X.; Garrett, B. C.; Tobias, D. J. *J. Am. Chem. Soc.* **2004**, *126*, 16308−16309.
(60) Sander, R. Compilation of Henrys Law Constants for Inorganic and Organic Species of Potential Importance in Environmental Chemistry, Version 3, 1999, http://www.henrys-law.org/henry.pdf.
(61) Nicholls, A.; Mobley, D. L.; Guthrie, J. P.; Chodera, J. D.; Bayly, C. I.; Cooper, M. D.; Pande, V. S. *J. Med. Chem.* **2008**, *51*, 769−779.
(62) Guthrie, J. P. *J. Phys. Chem. B* **2009**, *113*, 4501−4507.
(63) Geballe, M. T.; Skillman, A. G.; Nicholls, A.; Guthrie, J. P.; Taylor, P. J. *J. Comput.-Aided Mol. Des.* **2010**, *24*, 259−279.
(64) Linstrom, P., Mallard, W., Eds. *NIST Chemistry WebBook*; National Institute of Standards and Technology: Gaithersburg, MD, 2010, http://webbook.nist.gov/chemistry/.
(65) Tang, K. E.; Bloomfield, V. A. *Biophys. J.* **2000**, *79*, 2222−2234.
(66) Graziano, G. *Chem. Phys. Lett.* **2007**, *440*, 221−223.
(67) Mintz, C.; Gibbs, J.; Acree, W. E.; Abraham, M. H. *Thermochim. Acta* **2009**, *484*, 65−69.
(68) Stephens, T. W.; Chou, V.; Quay, A. N.; Acree, W. E., Jr.; Abraham, M. H. *Thermochim. Acta* **2011**, *519*, 103−113.
(69) Stephens, T. W.; De La Rosa, N. E.; Saifullah, M.; Ye, S.; Chou, V.; Quay, A. N.; Acree, W. E., Jr; Abraham, M. H. *Thermochim. Acta* **2011**, *523*, 214−220.
(70) Balakrishnan, G.; Sahoo, S. K.; Chowdhury, B. K.; Umapathy, S. *Faraday Discuss.* **2010**, *145*, 443−466.
(71) Rice, S. Diffusion-Controlled Reactions in Solution. In *Comprehensive Chemical Kinetics*; Bamford, C., Tipper, C., Eds.; Elsevier B.V.: Amsterdam, The Netherlands, 1985; Chapter 2, pp 3−45.
(72) Makitra, R. G.; Turovsky, A. A.; Zaikov, G. E. *Linear Energy Relationships to Chemical Kinetics*, 1st ed.; Nova Science Publishers: Hauppauge NY, USA, 2009.
(73) Koner, A.; Pischel, U.; Nau, W. *Org. Lett.* **2007**, *9*, 2899−2902.
(74) Jha, M.; Pratt, D. A. *Chem. Commun.* **2008**, *10*, 1252−1254.
(75) Avila, D. V.; Ingold, K. U.; Lusztyk, J.; Green, W. H.; Procopio, D. R. *J. Am. Chem. Soc.* **1995**, *117*, 2929−2930.
(76) MacFaul, P. A.; Ingold, K. U.; Lusztyk, J. *J. Org. Chem.* **1996**, *61*, 1316−1321.
(77) Snelgrove, D. W.; Lusztyk, J.; Banks, J. T.; Mulder, P.; Ingold, K. U. *J. Am. Chem. Soc.* **2001**, *123*, 469−477.
(78) Litwinienko, G.; Ingold, K. *Acc. Chem. Res.* **2007**, *40*, 222−230.
(79) Avila, D. V.; Brown, C. E.; Ingold, K. U.; Lusztyk, J. *J. Am. Chem. Soc.* **1993**, *115*, 466−470.
(80) Tsentalovich, Y. P.; Kulik, L. V.; Gritsan, N. P.; Yurkovskaya, A. V. *J. Phys. Chem. A* **1998**, *102*, 7975−7980.
(81) Tsentalovich, Y. P.; Fischer, H. *J. Chem. Soc., Perkin Trans. 2* **1994**, 729−733.
(82) Zytowski, T.; Fischer, H. *J. Am. Chem. Soc.* **1996**, *118*, 437−439.
(83) Lalevee, J.; Allonas, X.; Fouassier, J. P.; Rinaldi, D.; Lopez, M. F. R.; Rivail, J. L. *Chem. Phys. Lett.* **2005**, *415*, 202−205.
(84) Howard, J. A.; Ingold, K. U. *Can. J. Chem.* **1964**, *42*, 1044−1056.
(85) Howard, J. A.; Ingold, K. U. *Can. J. Chem.* **1964**, *42*, 1250−1253.
(86) Niki, E.; Kamiya, Y.; Ohta, N. *Bull. Chem. Soc. Jpn.* **1969**, *42*, 3224−3229.
(87) Frisch, M. J.; et al. *Gaussian 03*, revision C.02; Gaussian, Inc.: Wallingford, CT, 2004.
(88) Ho, J.; Klamt, A.; Coote, M. L. *J. Phys. Chem. A* **2010**, *114*, 13442−13444.
(89) Takano, Y.; Houk, K. N. *J. Chem. Theory Comput.* **2005**, *1*, 70−77.
(90) Sharma, S.; Harper, M. R.; Green, W. H. CanTherm v1.0. https://github.com/GreenGroup/CanTherm.
(91) Kulkarni, M. G.; Mashelkar, R. A.; Doraiswamy, L. K. *Chem. Eng. Sci.* **1980**, *35*, 823−830.
(92) Kulkarni, M. G.; Mashelkar, R. A. *AIChE J.* **1981**, *27*, 716−724.
(93) Denisov, E. T.; Denisova, T. G.; Pokidova, T. S. *Handbook of Free Radical Initiators*; John Wiley and Sons, Ltd: Hoboken, NJ, USA, 2003.
(94) Niki, E.; Kamiya, Y.; Ohta, N. *Bull. Chem. Soc. Jpn.* **1969**, *42*, 3220−3223.

(95) Makitra, R. G.; Polyuzhin, I. P.; Golovata, I. P. *Russ. J. Gen. Chem.* **2005**, *75*, 172−176.
(96) Abboud, J. L. M.; Notario, R. *Pure Appl. Chem.* **1999**, *71*, 645−718.
(97) Baulch, D. L.; Cobos, C. J.; Cox, R. A.; Frank, P.; Hayman, G.; Just, T.; Kerr, J. A.; Murrells, T.; Pilling, M. J.; Troe, J.; et al. *J. Phys. Chem. Ref. Data* **1994**, *23*, 847−848.
(98) Carstensen, H.-H.; Dean, A. M.; Deutschmann, O. *Proc. Combust. Inst.* **2007**, *31*, 149−157.
(99) Werner, H.-J.; Knowles, P. J.; Knizia, G.; Manby, F. R.; Schütz, M.; et al. MOLPRO, version 2010.1, a package of ab initio programs. see http://www.molpro.net.
(100) Lucarini, M.; Pedulli, G. F.; Valgimigli, L. *J. Org. Chem.* **1998**, *63*, 4497−4499.
(101) Bietti, M.; Salamone, M. *Org. Lett.* **2010**, *12*, 3654−3657.
(102) Salamone, M.; Giammarioli, I.; Bietti, M. *J. Org. Chem.* **2011**, 4645−4651.
(103) Valgimigli, L.; Banks, J. T.; Ingold, K.; Lusztyk, J. *J. Am. Chem. Soc.* **1995**, *117*, 9966−9971.
(104) Bietti, M.; Salamone, M.; DiLabio, G. A.; Jockusch, S.; Turro, N. J. *J. Org. Chem.* **2012**, *77*, 1267−1272.
(105) Abraham, M. H.; Grellier, P. L.; Prior, D. V.; Morris, J. J.; Taylor, P. J. *J. Chem. Soc., Perkin Trans. 2* **1990**, 521−529.
(106) Abraham, M. H.; Acree, W. E. *Green Chem.* **2006**, *8*, 906−915.
(107) Sprunger, L. M.; Proctor, A.; Acree, W. E.; Abraham, M. H. *Phys. Chem. Liq.* **2008**, *46*, 574−585.
(108) Howard, J. A. Homogeneous Liquid-Phase Autoxidations. In *Free Radicals*; Kochi, J., Ed.; John Wiley and Sons, Ltd: Hoboken, NJ, USA, 1973; Vol 2, Chapter 12, pp 3−62.
(109) Hendry, D. G.; Russell, G. A. *J. Am. Chem. Soc.* **1964**, *86*, 2368−2371.
(110) Howard, J. A.; Ingold, K. U. *Can. J. Chem.* **1966**, *44*, 1119−1130.
(111) Bennett, J. E.; Brunton, G.; Smith, J. R. L.; Salmon, T. M. F.; Waddington, D. J. *J. Chem. Soc., Faraday Trans. 1* **1987**, *83*, 2433−2447.
(112) Kaloerova, V. G.; Nikolaevskii, A. N.; Kucher, R. V.; Batrak, T. A. *Dokl. Akad. Nauk SSSR* **1978**, *242*, 641−644.
(113) Galano, A. *J. Phys. Chem. A* **2007**, *111*, 5086−5091.
(114) Asatryan, R.; Bozzelli, J. W. *Phys. Chem. Chem. Phys.* **2008**, *10*, 1769−1780.
(115) Wang, L. M.; Zhang, J. S. *Chem. Phys. Lett.* **2002**, *356*, 490−496.
(116) Kukui, A.; Borissenko, D.; Laverdet, G.; Le Bras, G. *J. Phys. Chem. A* **2003**, *107*, 5732−5742.
(117) Tully, F. P.; Ravishankara, A. R.; Thompson, R. L.; Nicovich, J. M.; Shah, R. C.; Kreutter, N. M.; Wine, P. H. *J. Phys. Chem.* **1981**, *85*, 2262−2269.
(118) Villano, S. M.; Huynh, L. K.; Carstensen, H.-H.; Dean, A. M. *J. Phys. Chem. A* **2012**, *116*, 5068−5089.
(119) Villano, S. M.; Huynh, L. K.; Carstensen, H.-H.; Dean, A. M. *J. Phys. Chem. A* **2011**, *115*, 13425−13442.
(120) Fernandes, R. X.; Zador, J.; Jusinski, L. E.; Miller, J. A.; Taatjes, C. A. *Phys. Chem. Chem. Phys.* **2009**, *11*, 1320−1327.
(121) Battino, R.; Rettich, T. R.; Tominaga, T. *J. Phys. Chem. Ref. Data* **1983**, *12*, 163−178.